
PARSIMONIOUS PHYSICS-INFORMED RANDOM PROJECTION NEURAL NETWORKS FOR INITIAL-VALUE PROBLEMS OF ODES AND INDEX-1 DAEs

A PREPRINT

Gianluca Fabiani

Scuola Superiore Meridionale
Università degli Studi di Napoli Federico II
Italy
gianluca.fabiani@unina.it

Evangelos Galaris

Dept. of Mathematics and Applications
Università degli Studi di Napoli Federico II,
Italy
evangelos.galaris@unina.it

Lucia Russo

Scienze e Tecnologie per l'Energia e la Mobilità Sostenibili
Consiglio Nazionale delle Ricerche
Italy
lucia.russo@stems.cnr.it

Constantinos Siettos*

Dept. of Mathematics and Applications,
Scuola Superiore Meridionale
Università degli Studi di Napoli "Federico II"
Italy
constantinos.siettos@unina.it

March 14, 2022

ABSTRACT

We address a physics-informed neural network based on the concept of random projections for the numerical solution of initial value problems of nonlinear ODEs in linear-implicit form and index-1 DAEs, which may also arise from the spatial discretization of PDEs. The proposed scheme has a single hidden layer with appropriately randomly parametrized Gaussian kernels and a linear output layer, while the internal weights are fixed to ones. The unknown weights between the hidden and output layer are computed by Newton's iterations, using the Moore-Penrose pseudoinverse for low to medium scale, and sparse QR decomposition with L^2 regularization for medium to large scale systems. To deal with stiffness and sharp gradients, we thus propose an variable step size scheme based on the elementary local error control algorithm for adjusting the step size of integration and address a natural continuation method for providing good initial guesses for the Newton iterations. Building on previous works on random projections, we prove the approximation capability of the scheme for ODEs in the canonical form and index-1 DAEs in the semiexplicit form. The "optimal" bounds of the uniform distribution from which the values of the shape parameters of the Gaussian kernels are sampled are "parsimoniously" chosen based on the bias-variance trade-off decomposition, thus using the stiff van der Pol model as the reference solution for this task. The optimal bounds are fixed once and for all the problems studied here. In particular, the performance of the scheme is assessed through seven benchmark problems. Namely, we considered four index-1 DAEs, the Robertson model, a no autonomous model of five DAEs describing the motion of a bead on a rotating needle, a non autonomous model of six DAEs describing a power discharge control problem, the chemical so-called Akzo Nobel problem and three stiff problems, the Belousov-Zhabotinsky model, the Allen-Cahn PDE phase-field model and the Kuramoto-Sivashinsky PDE giving rise to chaotic dynamics. The efficiency of the scheme in terms of both numerical accuracy and computational cost is compared with three stiff/DAE solvers (ode23t, ode23s, ode15s) of the MATLAB ODE suite. Our results show that, the proposed scheme outperforms the aforementioned stiff solvers in several

*Corresponding author

cases, especially in regimes where high stiffness and/or sharp gradients arise, in terms of numerical accuracy, while the computational costs are for any practical purposes comparable.

Keywords Physics-Informed Machine Learning · Initial Value Problems · Differential-Algebraic Equations · Random Projection Neural Networks

1 Introduction

The interest in using machine learning as an alternative to the classical numerical analysis methods [26, 11, 25, 65] for the solution of the inverse [42, 50, 14, 29, 69, 68, 1], and forward problems [46, 21, 52, 27, 44] in differential equations modelling dynamical systems can be traced back three decades ago. Today, this interest has been boosted together with our need to better understand and analyse the emergent dynamics of complex multiphysics/ multiscale dynamical systems of fundamental theoretical and technological importance [40]. The objectives are mainly two. First, that of the solution of the inverse problem, i.e. that of identifying/discovering the hidden macroscopic laws, thus learning nonlinear operators and constructing coarse-scale dynamical models of ODEs and PDEs and their closures, from microscopic large-scale simulations and/or from multi-fidelity observations [10, 57, 58, 59, 62, 9, 3, 47, 74, 15, 16, 48]. Second, based on the constructed coarse-scale models, to systematically investigate their dynamics by efficiently solving the corresponding differential equations, especially when dealing with (high-dimensional) PDEs [24, 13, 15, 16, 22, 23, 38, 49, 59, 63]. Towards this aim, physics-informed machine learning [57, 58, 59, 48, 53, 15, 16, 40] has been addressed to integrate available/incomplete information from the underlying physics, thus relaxing the “curse of dimensionality”. However, failures may arise at the training phase especially in deep learning formulations, while there is still the issue of the corresponding computational cost [45, 75, 76, 40]. Thus, a bet and a challenge is to develop physics-informed machine learning methods that can achieve high approximation accuracy at a low computational cost.

Within this framework, and towards this aim, we propose a physics-informed machine learning (PIRPNN) scheme based on the concept of random projections [39, 56, 30], for the numerical solution of initial-value problems of nonlinear ODEs and index-1 DAEs as these may also arise from the spatial discretization of PDEs. Our scheme consists of a single hidden layer, with Gaussian kernels, in which the weights between the input and hidden layer are fixed to ones. The shape parameters of the Gaussian kernels are random variables drawn from a uniform distribution which bounds are “parsimoniously” chosen based on the expected bias-variance trade-off [6]. The unknown parameters, i.e. the weights between the hidden and the output layer are estimated by solving with Newton-type iterations a system of nonlinear algebraic equations. For low to medium scale systems this is achieved using SVD decomposition, while for large scale systems, we exploit a sparse QR factorization algorithm with L^2 regularization [18]. Furthermore, to facilitate the convergence of Newton’s iterations, especially at very stiff regimes and regimes with very sharp gradients, we (a) propose a variable step size scheme for adjusting the interval of integration based on the elementary local error control algorithm [71], and (b) address a natural continuation method for providing good initial guesses for the unknown weights. To demonstrate the performance of the proposed method in terms of both approximation accuracy and computational cost, we have chosen seven benchmark problems, four index-1 DAEs and three stiff problems of ODEs, thus comparing it with the ode23s, ode23t and ode15s solvers of the MATLAB suite ODE [65]. In particular, we considered the index-1 DAE Robertson model describing the kinetics of an autocatalytic reaction [60, 66], an index-1 DAEs model describing the motion of a bead on a rotating needle [66], an index-1 DAEs model describing the dynamics of a power discharge control problem [66], the index-1 DAE chemical Akzo Nobel problem [51, 72], the Belousov-Zhabotinsky chemical kinetics stiff ODEs [7, 77], the Allen-Chan phase-field PDE describing the process of phase separation for generic interfaces [2] and Kuramoto-Sivashinsky PDE [43, 70, 73]. The PDEs are discretized in space with central finite differences, thus resulting to a system of stiff ODEs [73]. The results show that the proposed scheme outperforms the aforementioned solvers in several cases in terms of numerical approximation accuracy, especially in problems where stiffness and sharp gradients arise, while the required computational times are comparable for any practical purposes.

2 Methods

First, we describe the problem, and present some preliminaries on the use of machine learning for the solution of differential equations and on the concept of random projections for the approximation of continuous functions. We then present the proposed physics-informed random projection neural network scheme, and building on previous works [56], we prove that in principle the proposed PIRPNN can approximate with any given accuracy any unique continuously differentiable function that satisfies the Picard-Lindelöf Theorem. Finally, we address (a) a variable step size scheme for adjusting the interval of integration and (b) a natural continuation method, to facilitate the convergence of Newton iterations, especially in regimes where stiffness and very sharp gradients arise.

2.1 Description of the Problem

We focus on IVPs of ODEs and index-1 DAEs that may also arise from the spatial discretization of PDEs using for example finite differences, finite elements and spectral methods. In particular, we consider IVPs in the linear implicit form of:

$$\mathbf{M} \frac{d\mathbf{u}(t)}{dt} = \mathbf{f}(t, \mathbf{u}(t)), \quad \mathbf{u}(0) = \mathbf{z}. \quad (1)$$

$\mathbf{u} \in \mathbb{R}^m$ denotes the set of the states $\{u_1, u_2, \dots, u_i, \dots, u_m\}$, $\mathbf{M} \in \mathbb{R}^{m \times m}$ is the so-called mass matrix with elements M_{ij} , $\mathbf{f} : \mathbb{R} \times \mathbb{R}^m \rightarrow \mathbb{R}^m$ denotes the set of Lipschitz continuous multivariate functions, say $f_i(t, u_1, u_2, \dots, u_m)$ in some closed domain D , and $\mathbf{z} \in \mathbb{R}^m$ are the initial conditions. When $\mathbf{M} = \mathbf{I}$, the system reduces to the canonical form. The above formulation includes problems of DAEs when \mathbf{M} is a singular matrix, including semiexplicit DAEs in the form [66]:

$$\begin{aligned} \frac{d\mathbf{u}(t)}{dt} &= \mathbf{f}(t, \mathbf{u}(t), \mathbf{v}(t)), & \mathbf{u}(0) &= \mathbf{z}, \\ \mathbf{0} &= \mathbf{g}(t, \mathbf{u}(t), \mathbf{v}(t)), \end{aligned} \quad (2)$$

where, we assume that the Jacobian $\nabla_{\mathbf{v}} \mathbf{g}$ is nonsingular, $\mathbf{f} : \mathbb{R} \times \mathbb{R}^{m-l} \times \mathbb{R}^l \rightarrow \mathbb{R}^{m-l}$, $\mathbf{g} : \mathbb{R} \times \mathbb{R}^{m-l} \times \mathbb{R}^l \rightarrow \mathbb{R}^l$.

In this work, we use physics-informed random projection neural networks for the numerical solution of the above type of IVPs which solutions are characterized both by sharp gradients and stiffness [64, 66].

Stiff problems are the ones which integration “with a code that aims at non stiff problems proves conspicuously inefficient for no obvious reason (such a severe lack of smoothness in the equation or the presence of singularities)” [64]. At this point, it is worthy to note that stiffness is not connected to the presence of sharp gradients [64]. For example, at the regimes where the relaxation oscillations of the van der Pol model exhibit very sharp changes resembling discontinuities, the equations are not stiff.

2.2 Physics-informed machine learning for the solution of differential equations

Let’s assume a set of n_x points $\mathbf{x}_i \in \Omega \subset \mathbb{R}^d$ of the independent (spatial) variables, thus defining the size grid in the domain Ω , $n_{\partial\Omega}$ points along the boundary $\partial\Omega$ of the domain and n_t points in the time interval, where the solution is sought. For our illustrations, let’s consider a time-dependent PDE in the form of

$$\frac{\partial u}{\partial t} = L(\mathbf{x}, u, \nabla u, \nabla^2 u, \dots), \quad (3)$$

where L is the partial differential operator acting on u satisfying the boundary conditions $Bu = g$, in $\partial\Omega$, where B is the boundary differential operator. Then, the solution with machine learning of the above PDE involves the solution of a minimization problem of the form:

$$\begin{aligned} \min_{\mathbf{P}, \mathbf{Q}} E(\mathbf{P}, \mathbf{Q}) &:= \sum_{i=1}^{n_x} \sum_{j=1}^{n_t} \left\| \frac{d\Psi}{dt}(\cdot) - L(\mathbf{x}_i, \Psi(\cdot), \nabla\Psi(\cdot), \nabla^2\Psi(\cdot), \dots) \right\|^2 + \\ &\sum_{j=1}^{n_{\partial\Omega}} \|B\Psi(\cdot) - g\|^2, \end{aligned} \quad (4)$$

where $\Psi(\cdot) := \Psi(\mathbf{x}_i, t_j, \mathcal{N}(\mathbf{x}_i, t_j, \mathbf{P}, \mathbf{Q}))$ represents a machine learning constructed function approximating the solution u at \mathbf{x}_i at time t_j and $\mathcal{N}(\mathbf{x}_i, t_j, \mathbf{P}, \mathbf{Q})$ is a machine learning algorithm; \mathbf{P} contains the parameters of the machine learning scheme (e.g. for a FNN the internal weights \mathbf{W} , the biases \mathbf{B} , the weights between the last hidden and the output layer \mathbf{W}^o), \mathbf{Q} contains the hyper-parameters (e.g. the parameters of the activation functions for a FNN, the learning rate, etc.). In order to solve the optimization problem (4), one usually needs quantities such as the derivatives of $\mathcal{N}(\mathbf{x}, \mathbf{P}, \mathbf{Q})$ with respect to t, \mathbf{x} and the parameters of the machine learning scheme (e.g. the weights and biases for a FNN). These can be obtained in several ways, numerically using finite differences or other approximation schemes, or by symbolic or automatic differentiation [5, 49]). The above approach can be directly implemented also for solving systems of ODEs as these may also arise by discretizing in space PDEs. Yet, for large scale problems even for the simple case of single layer networks, when the number of hidden nodes is large enough, the solution of the above optimization problem is far from trivial. Due to the “curse of dimensionality” the computational cost is high, while when dealing with differential equations which solutions exhibit sharp gradients and/or stiffness several difficulties or even failures in the convergence have been reported [45, 75, 76].

2.3 Random Projection Neural Networks

Random projection neural networks (RPNN) including Random Vector Functional Link Networks (RVFLNs) [36, 35], Echo-State Neural Networks and Reservoir Computing [37], and Extreme Learning Machines [34, 33] have been introduced to tackle the ‘‘curse of dimensionality’’ encountered at the training phase. One of the fundamental works on random projections is the celebrated Johnson and Lindenstrauss Lemma [39] stating that for a matrix $\mathbf{W} \in \mathbb{R}^{d \times n}$ containing n , \mathbf{w} points in \mathbb{R}^d , there exists a projection $\mathbf{F} : \mathbb{R}^d \rightarrow \mathbb{R}^k$ defined as:

$$\mathbf{F}(\mathbf{w}) = \frac{1}{\sqrt{k}} \mathbf{R}\mathbf{w}, \quad (5)$$

where $\mathbf{R} = [r_{ij}] \in \mathbb{R}^{k \times d}$ has components which are i.i.d. random variables sampled from a normal distribution, which maps \mathbf{W} into a random subspace of dimension $k \geq O\left(\frac{\ln n}{\epsilon^2}\right)$, where the distance between any pair of points in the embedded space $\mathbf{F}(\mathbf{W})$ is bounded in the interval $[1 - \epsilon, 1 + \epsilon]$.

Regarding single layer feedforward neural networks (SLFNNs), in order to improve the approximation accuracy, Rosenblatt [61] suggested the use of randomly parametrized activation functions for single layer structures. Thus, the approximation of a sufficiently smooth function $f(\mathbf{x}) : \mathbb{R}^d \rightarrow \mathbb{R}$ is written as a linear combination of appropriately randomly parametrized family of N basis functions $\phi_i : \mathbb{R} \times \mathbb{R}^p \rightarrow \mathbb{R}$ as

$$f(\mathbf{x}) \simeq f_N(\mathbf{x}) = \sum_{i=1}^N w_i^o \phi_i(\mathbf{w}_i^T \mathbf{x} + b_i, \mathbf{p}_i), \quad (6)$$

where $\mathbf{w}_i \in \mathbb{R}^d$ are the weighting coefficients of the inputs, $b \in \mathbb{R}$ are the biases and $\mathbf{p}_i \in \mathbb{R}^p$ are the shape parameters of the basis functions.

More generally, for SLFNNs with d inputs, k outputs and N neurons in the hidden layer, the random projection of n samples in the d -dimensional input space \mathbf{X} can be written in a matrix-vector notation as:

$$\mathbf{Y}_N = \mathbf{\Phi}_N \mathbf{W}^o, \quad \mathbf{Y} \in \mathbb{R}^{n \times k}, \quad (7)$$

where, $\mathbf{\Phi}_N \in \mathbb{R}^{n \times N}$ is a random matrix containing the outputs of the hidden layer as shaped by the n samples in the d -dimensional space, the randomly parametrized internal weights $\mathbf{W} \in \mathbb{R}^{d \times N}$, the biases $\mathbf{b} \in \mathbb{R}^N$ and shape parameters of the N activation functions; $\mathbf{W}^o \in \mathbb{R}^{N \times k}$ is the matrix containing the weights w_{ij}^o between the hidden and the output layer.

In the early '90s, Barron [4] proved that for functions with integrable Fourier transformations, a random sample of the parameters of sigmoidal basis functions from an appropriately chosen distribution results to an approximation error of the order of $1/N$. Igel'nik and Pao [36] extending Barron's proof [4] for any family of L^2 integrable basis functions ϕ_i proved the following theorem for RVFLNs:

Theorem 2.1. SLFNNs as defined by Eq.(6) with weights \mathbf{w}_i and biases b_i selected randomly from a uniform distribution and for any family of L^2 integrable basis functions ϕ_i , are universal approximators of any Lipschitz continuous function f defined in the standard hypercube I^d and the expected rate of convergence of the approximation error, i.e., the distance between $f(\mathbf{x})$ and $f_N(\mathbf{x})$ on any compact set $K \subset I^d$ defined as:

$$\rho^2(f(\mathbf{x}), f_N(\mathbf{x})) = \mathbb{E} \left[\int_K (f(\mathbf{x}) - f_N(\mathbf{x}))^2 d\mathbf{x} \right] \quad (8)$$

is of the order of (C/\sqrt{N}) , where $C = C(f, \phi_i, \beta, \Omega, \alpha, d)$; \mathbb{E} denotes expectation over a probabilistic space $S(\mathcal{U}, \alpha)$, β is the support of ϕ_i in $\prod_{i=1}^d (-\beta \mathbf{w}_i, \beta \mathbf{w}_i)$.

Similar results for one-layer schemes have been also reported in other studies (see e.g. [56, 30]). Rahimi and Recht [56] proved the following Theorem:

Theorem 2.2. Let p be a probability distribution drawn i.i.d. on \mathcal{U} and consider the basis functions $\phi(x, \alpha) : \mathcal{X} \times \mathcal{U} \rightarrow \mathbb{R}$ that satisfy $\sup_{x, \alpha} \phi(x, \alpha) \leq 1$. Define the set of functions

$$\mathcal{S}_p \equiv \left\{ f(x) = \int w(\alpha) \phi(x; \alpha) d\alpha, |w(\alpha)| \leq Cp(\alpha) \right\}, \quad (9)$$

and let μ be a measure on \mathcal{X} . Then, if one takes a function f in \mathcal{S}_p , and N values $\alpha_1, \alpha_2, \dots, \alpha_N$ of the shape parameter α are drawn i.i.d. from p , for any $\delta > 0$ with probability at least $1 - \delta$ over $\alpha_1, \alpha_2, \dots, \alpha_N$, there exists a function defined as $f_N = \sum_{j=1}^N w_j \phi_j(x; \alpha_j)$, $|w_j| \leq \frac{C}{N}$ so that

$$\int_{\mathcal{X}} (f(x), f_N(x))^2 d\mu(x) \leq \frac{C}{\sqrt{N}} \left(1 + \sqrt{2 \log \frac{1}{\delta}}\right). \quad (10)$$

For the so-called Extreme-Learning machines (ELMs), which similarly to RVFLNs are FNNs with randomly assigned internal weights and biases of the hidden layers, Huang et al. [34, 33] has proved the following theorem:

Theorem 2.3. For any set of n input-output pairs $(\mathbf{x}_i, \mathbf{y}_i), i = 1, 2, \dots, N$ ($\mathbf{x}_i \in \mathbb{R}^d, \mathbf{y}_i \in \mathbb{R}^k$), the projection matrix $\Phi_N \in \mathbb{R}^{N \times N}$ in Eq.(7) is invertible and

$$\|\Phi_N \mathbf{W}^o - \mathbf{Y}_N\| = 0, \quad (11)$$

with probability 1 for $N = n$, \mathbf{W}, \mathbf{b} randomly chosen from any probability distribution, and an activation function that is infinitely differentiable.

2.4 The Proposed Physics-Informed RPNN-based method for the solution of ODEs and index-1 DAEs

Here, we propose a physics-informed machine learning method based on random projections for the solution of IVPs of a system given by Eq.(1)/(2) in n collocation points in an interval, say $[t_0 \ t_{end}]$. According to the previous notation, for this problem we have $d = k = 1$. Thus, Eq.(7) reads:

$$\mathbf{Y}_N = \Phi_N \mathbf{w}^o, \quad \mathbf{Y}_N \in \mathbb{R}^n, \quad \Phi_N \in \mathbb{R}^{n \times N}, \quad \mathbf{w}^o \in \mathbb{R}^N \quad (12)$$

Thus, the output of the RPNN is spanned by the range $\mathcal{R}(\Phi)$, i.e. the column vectors of Φ_N , say $\phi_i \in \mathbb{R}^n$. Hence, the output of the RPNN can be written as:

$$\mathbf{Y}_N = \sum_{i=1}^N w_i^o \phi_i \quad (13)$$

For an IVP of m variables, we construct m such PIRPNNs. We denote by $\Psi(t, \mathbf{W}, \mathbf{W}^o, \mathbf{P})$ the set of functions $\Psi_{Ni}(t, \mathbf{w}_i^o, \mathbf{p}_i), i = 1, 2, \dots, m$ that approximate the solution profile u_i at time t , defined as:

$$\Psi_{Ni}(t, \mathbf{w}_i, \mathbf{w}_i^o, \mathbf{p}_i) = z_i + (t - t_0) \mathbf{w}_i^{oT} \Phi_{Ni}(t, \mathbf{w}_i, \mathbf{p}_i), \quad (14)$$

where $\Phi_{Ni}(t, \mathbf{w}_i, \mathbf{p}_i) \in \mathbb{R}^N$ is the column vector containing the values of the N basis functions at time t as shaped by \mathbf{w}_i and \mathbf{p}_i containing the values of the parameters of the N basis functions and $\mathbf{w}_i^o = [w_{1i}^o \ w_{2i}^o \ \dots \ w_{Ni}^o]^T \in \mathbb{R}^N$ is the vector containing the values of the output weights of the i -th PIRPNN network. Note that the above set of functions are continuous functions of t and satisfy explicitly the initial conditions.

For index-1 DAEs, with say $M_{ij} = 0, \forall i \geq l, j = 1, 2, \dots, m$, or in the semiexplicit form of (2), there are no explicit initial conditions z_i for the variables $u_i, i = l, l+1, \dots, m$, or the variables \mathbf{v} in (2): these values have to satisfy the constraints $f_i(t, \mathbf{u}) = 0, i \geq l$, (equivalently $\mathbf{0} = \mathbf{g}(t, \mathbf{u}, \mathbf{v}) \forall t$, thus one has to start with consistent initial conditions. Assuming that the corresponding Jacobian matrix of the $f_i(t, \mathbf{u}) = 0, i = l, l+1, \dots, m$ with respect to u_i , and for the semiexplicit form (2), $\nabla_{\mathbf{v}} \mathbf{g}$, is not singular, one has to solve initially at $t = 0$, using for example Newton-Raphson iterations, the above nonlinear system of $m - l$ algebraic equations in order to find a consistent set of initial values. Then, one can write the approximation functions of the $u_i, i = k, k+1, \dots, m/\mathbf{v}$ variables as in Eq.(14).

With n collocation points in $[t_0 \ t_{end}]$, by fixing the values of the interval weights \mathbf{w}_i and the shape parameters \mathbf{p}_i , the loss function that we seek to minimize with respect to the unknown coefficients \mathbf{w}_i^o is given by:

$$\mathcal{L}(\mathbf{W}^o) = \sum_{j=1}^n \left(M \frac{d\Psi}{dt}(t_j, \mathbf{W}, \mathbf{W}^o, \mathbf{P}) - \mathbf{f}(t_j, \Psi(t_j, \mathbf{W}, \mathbf{W}^o, \mathbf{P})) \right)^2, \quad (15)$$

When the system of ODEs/DAEs results from the spatial discretization of PDEs, we assume that the corresponding boundary conditions have been appropriately incorporated into the resulting algebraic equations explicitly or otherwise can be added in the loss function as algebraic constraints.

Based on the above notation, we construct m PIRPNNs, taking, for each network \mathcal{N}_i, N Gaussian RBFs which, for $j = 1, \dots, N, i = 1, \dots, m$, are given by:

$$g_{ji}(t, w_{ji}, b_{ji}, \alpha_{ji}, c_j) = e^{-\alpha_{ji}(w_{ji}t + b_{ji} - c_j)^2}. \quad (16)$$

The values of the (hyper) parameters, namely w_{ji}, b_{ji}, c_j are set as:

$$w_{ji} = 1, \quad b_{ji} = 0, \quad c_j = t_j = t_0 + (j-1) \frac{t_{end} - t_0}{N-1},$$

while the values of the shape parameters $\alpha_{ji} > 0$ are sampled from an appropriately chosen uniform distribution. Under the above assumptions, the time derivative of Ψ_{Ni} is given by:

$$\frac{d\Psi_{Ni}}{dt} = \sum_{j=1}^N w_{ji}^o e^{-\alpha_{ji}(t-t_j)^2} - 2(t-t_0) \sum_{j=1}^N \alpha_{ji} w_{ji}^o (t-t_j) e^{-\alpha_{ji}(t-t_j)^2}. \quad (17)$$

2.4.1 Approximation with the PIRPNN

At this point, we note that in Theorems 2.1 and 2.3, the universal approximation property is based on the random base expansion given by Eq.(6), while in our case, we have a slightly different expansion given by Eq.(14). Here, we show that the PIRPNN given by Eq.(14) is a universal approximator of the solution \mathbf{u} of the ODEs in canonical form or of the index-1 DAEs in the semiexplicit form (2).

Proposition 1. For the IVP problem (1) in the canonical form or in the semiexplicit form (2), the PIRPNN solution Ψ_{Ni} given by Eq.(14) with N Gaussian basis functions defined by Eq.(16), and the values of the shape parameters α_{ji} drawn i.i.d. from a uniform distribution converges uniformly to the solution profile $\mathbf{u}(t)$ in a closed time interval $[t_0 \ t_{end}]$.

Proof. Assuming that the system in Eq.(1) can be written in the canonical form, the Picard-Lindelöf Theorem [17] holds true, then it exists a unique continuously differentiable function defined on a closed time interval $[t_0 \ t_{end}]$ given by:

$$u_i(t) = z_i + \int_{t_0}^t f_i(s, \mathbf{u}(s))ds, \quad i = 1, 2, \dots, m \quad (18)$$

From Eq.(14) we have:

$$\Psi_{Ni}(t) = z_i + (t - t_0) \sum_{j=1}^N w_j^o e^{-\alpha_j(t-t_j)^2}. \quad (19)$$

By the change of variables, $\tau = \frac{s-t_0}{t-t_0}$, the integral in Eq.(18) becomes

$$\int_{t_0}^t f_i(s, \mathbf{u}(s))ds = (t - t_0) \int_0^1 f_i(\tau(t-t_0) + t_0, \mathbf{u}(\tau(t-t_0) + t_0))d\tau. \quad (20)$$

Hence, by Eqs.(18),(19),(20), we have:

$$I_n(t) \equiv \int_0^1 f_i(\tau(t-t_0) + t_0, \mathbf{u}(\tau(t-t_0) + t_0))d\tau \approx \sum_{j=1}^N w_j^o e^{-\alpha_j(t-t_j)^2}. \quad (21)$$

Thus, in fact, upon convergence, the PIRPNN provides an approximation of the normalized integral. By Theorem 3, we have that in the interval $[t_0 \ t_{end}]$, the PIRPNN with the shape parameter of the Gaussian kernel drawn i.i.d. from a uniform distribution provides, a uniform approximation of the integral in Eq.(18) in terms of a Monte Carlo integration method as also described in [36].

Hence, as the initial conditions are explicitly satisfied by $\Psi_{Ni}(t)$, we have from Eq.(10) an upper bound for the uniform approximation of the solution profile u_i with probability $1 - \delta$.

For index-1 DAEs in the semiexplicit form of (2), by the implicit function theorem, we have that the DAE system is *in principle* equivalent with the ODE system in the canonical form:

$$\frac{d\mathbf{u}(t)}{dt} = \mathbf{f}(t, \mathbf{u}(t), \mathcal{H}(t, \mathbf{u})), \quad (22)$$

where $\mathbf{v}(t) = \mathcal{H}(t, \mathbf{u}(t))$ is the unique solution of $\mathbf{0} = \mathbf{g}(t, \mathbf{u}(t), \mathbf{v}(t))$. Hence, in that case, the proof of convergence reduces to the one above for the ODE system in the canonical form. \square

2.4.2 Computation of the unknown weights

For n collocation points, the outputs of each network $\mathcal{N}_i \equiv \mathcal{N}_i(t_1, t_2, \dots, t_n, \mathbf{w}_i^o, \mathbf{p}_i) \in \mathbb{R}^n$, $i = 1, 2, \dots, m$, are given by:

$$\mathcal{N}_i = \mathbf{R}_i \mathbf{w}_i^o, \quad \mathbf{R}_i \equiv \mathbf{R}_i(t_1, \dots, t_n, \mathbf{p}_i) = \begin{bmatrix} g_{1i}(t_1) & \cdots & g_{Ni}(t_1) \\ \vdots & \vdots & \vdots \\ g_{1i}(t_n) & \cdots & g_{Ni}(t_n) \end{bmatrix}. \quad (23)$$

The minimization of the loss function (15) is performed over the nm nonlinear residuals F_q :

$$F_q(\mathbf{W}^o) = \sum_{j=1}^m M_{ij} \frac{d\Psi_{Nj}}{dt_l}(t_l, \mathbf{w}_j^o) - f_i(t_l, \Psi_{N1}(t_l, \mathbf{w}_1^o), \dots, \Psi_{Nm}(t_l, \mathbf{w}_m^o)), \quad (24)$$

where $q = l + (i - 1)n$, $i = 1, 2, \dots, m$, $l = 1, 2, \dots, n$, $\mathbf{W}^o \in \mathbb{R}^{mN}$ is the column vector obtained by collecting the values of all m vectors $\mathbf{w}_i^o \in \mathbb{R}^N$, $\mathbf{W}^o = [\mathbf{W}_k^o] = [\mathbf{w}_1^o, \mathbf{w}_2^o \dots, \mathbf{w}_m^o]^T$, $k = 1, 2, \dots, mN$. Thus, the solution to the above non-linear least squares problem can be obtained, e.g. with Newton-type iterations such as Newton-Raphson, Quasi-Newton and Gauss-Newton methods (see e.g. [20]). For example, by setting $\mathbf{F}(\mathbf{W}^o) = [F_1(\mathbf{W}^o) \dots F_q(\mathbf{W}^o) \dots F_{(nm)}(\mathbf{W}^o)]^T$, the new update $d\mathbf{W}^{o(\nu)}$ at the (ν) -th Gauss-Newton iteration is computed by the solution of the linearized system:

$$(\nabla_{\mathbf{W}^{o(\nu)}} \mathbf{F})^T \nabla_{\mathbf{W}^{o(\nu)}} \mathbf{F} \quad d\mathbf{W}^{o(\nu)} = -(\nabla_{\mathbf{W}^{o(\nu)}} \mathbf{F})^T \mathbf{F}(\mathbf{W}^{o(\nu)}), \quad (25)$$

where $\nabla_{\mathbf{W}^{o(\nu)}} \mathbf{F} \in \mathbb{R}^{nm \times mN}$ is the Jacobian matrix of \mathbf{F} with respect to $\mathbf{W}^{o(\nu)}$. Note that the residuals depend on the derivatives $\frac{\partial \Psi_{Ni}(\cdot)}{\partial t_l}$ and the approximation functions $\Psi_{Ni}(\cdot)$, while the elements of the Jacobian matrix depend on the derivatives of $\frac{\partial \Psi_{Ni}(\cdot)}{\partial w_{ji}^o}$ as well as on the mixed derivatives $\frac{\partial^2 \Psi_{Ni}(\cdot)}{\partial t_l \partial w_{ji}^o}$. Based on (17), the latter are given by

$$\frac{\partial^2 \Psi_{Ni}}{\partial t_l \partial w_{ji}^o} = \frac{\partial \mathcal{N}_i(t_l, \mathbf{w}_i^o, \mathbf{p}_i)}{\partial w_{ji}^o} - 2(t_l - t_0) \alpha_{ji} (t_l + b_{ji} - c_j) e^{(-\alpha_{ji}(t_l + b_{ji} - c_j)^2)}, \quad (26)$$

Based on the above, the elements of the Jacobian matrix $\nabla_{\mathbf{W}^{o(\nu)}} \mathbf{F}$ can be computed analytically as:

$$\frac{\partial F_p}{\partial W_q^o} = \frac{\sum_{j=1}^m M_{ij} \partial^2 \Psi_{Ni}(\cdot)}{\partial t_l \partial w_{jk}^o} - \frac{\partial f_i(t_l)}{\partial w_{jk}^o} \quad (27)$$

where, as before, $q = l + (i - 1)n$ and $p = j + (k - 1)h$.

However, in general, even when $N \geq n$, the Jacobian matrix is expected to be rank deficient, or nearly rank deficient, since some of the rows due to the random construction of the basis functions can be nearly linear dependent. Thus, the solution of the corresponding system, and depending on the size of the problem, can be solved using for example truncated SVD decomposition or QR factorization with regularization. The truncated SVD decomposition scheme results to the Moore-Penrose pseudoinverse and the updates $d\mathbf{W}^{o(\nu)}$ are given by:

$$d\mathbf{W}^{o(\nu)} = -(\nabla_{\mathbf{W}^{o(\nu)}} \mathbf{F})^\dagger \mathbf{F}(\mathbf{W}^{o(\nu)}), \quad (\nabla_{\mathbf{W}^{o(\nu)}} \mathbf{F})^\dagger = \mathbf{V}_\epsilon \Sigma_\epsilon^\dagger \mathbf{U}_\epsilon^T,$$

where Σ_ϵ^\dagger is the inverse of the diagonal matrix with singular values of $\nabla_{\mathbf{W}^o} \mathbf{F}$ above a certain value ϵ , and $\mathbf{U}_\epsilon, \mathbf{V}_\epsilon$ are the matrices with columns the corresponding left and right eigenvectors, respectively. If we have already derived $\nabla_{\mathbf{W}^{o(\tilde{\nu})}} \mathbf{F}$ at an iteration $\tilde{\nu} < \nu$, then in order to decrease the computational cost, one can proceed with a Quasi-Newton scheme, thus using the same pseudoinverse of the Jacobian for the next iterations until convergence, e.g., computing the SVD decomposition for only the first and second Newton-iterations and keep the same $(\nabla_{\mathbf{W}^{o(1)}} \mathbf{F})^\dagger$ for the next iterations.

For large-scale sparse Jacobian matrices, as those arising for example from the discretization of PDEs, one can solve the regularization problem using other methods such as sparse QR factorization. Here, to account for the ill-posed Jacobian, we have used a sparse QR factorization with regularization as implemented by SuiteSparseQR, a multifrontal multithreaded sparse QR factorization package [18, 19].

2.4.3 Parsimonious construction of the PIRPNN

The variable step size scheme. In order to deal with the presence of sharp gradients that resemble singularities at the time interval of interest, and stiffness, we propose an adaptive scheme for adjusting the step size of time integration as follows. The full time interval of integration $[t_0 \ t_{end}]$ is divided into sub-intervals, i.e., $[t_0 \ t_{end}] = [t_0 \ t_1] \cup [t_1 \ t_2] \cup \dots \cup [t_k \ t_{k+1}] \cup \dots \cup [t_{end-1} \ t_{end}]$, where $t_1, t_2, \dots, t_k, \dots, t_{end-1}$ are determined in an adaptive way. This decomposition of the interval leads to the solution of consecutive IVPs. In order to describe the variable step size scheme, let us assume that we have solved the problem up to interval $[t_{k-1} \ t_k]$, hence we have found $u_i^{(k-1)}$ and we are seeking $u_i^{(k)}$ in the current interval $[t_k \ t_{k+1}]$ with a width of $\Delta t_k = t_{k+1} - t_k$. Moreover suppose that the Quasi-Newton iterations after a certain number of iterations, say, $\nu \leq \nu_{max}$ (here $\nu_{max} = 5$) the resulting approximation error is [26, 71]:

$$err = \left\| \frac{\mathbf{F}(\mathbf{W}^{o(\nu)})}{AbsTol + RelTol \cdot \frac{d\Psi^{(k)}}{dt}} \right\|_{l^2}, \quad (28)$$

where $RelTol$ is the tolerance relative to the size of each derivative component $\frac{d\Psi_{Ni}^{(k)}}{dt}$ and $AbsTol$ is a threshold tolerance. Now, if $err < 1$ the solution is accepted, otherwise the solution is rejected.

In both cases, the size of the time interval will be updated according to the elementary local error control algorithm [71]:

$$\Delta t_k^* = 0.8\gamma \cdot \Delta t_k, \quad \text{with} \quad \gamma = \left(\frac{1}{err} \right)^{\frac{1}{\nu+1}}, \quad (29)$$

where γ is a scaling factor and 0.8 is a safe/conservative factor. Also Δt_k^* should not be allowed to increase or decrease too much, so γ should not be higher than a γ_{max} (here set to 4) and to be smaller than a γ_{min} (here set to 0.1).

Thus, if the Quasi-Newton scheme does not converge to a specific tolerance within a number of iterations ν_{max} , then the interval width is decreased, thus redefining a new guess $t_{k+1}^* = t_k + \Delta t_k^*$ for t_{k+1} and the Quasi-Newton scheme is repeated in the interval $[t_k \quad t_{k+1}^*]$.

Finally, the choice of the first subinterval $[t_0 \quad t_1]$ was estimated using an automatic detection code for selecting the starting step as described in [28, 32].

Regarding the interplay between the number of collocation points n and the time interval of integration as shaped by the variable step size scheme, we note that for band-limited profile solutions, according to the Nyquist sampling theorem, we can reconstruct the solution if the sampling rate is at least $2\nu_c$ samples per second; for n sampling points in a time interval say ΔT , the maximum allowed frequency for band-limited signals should not exceed $\nu_c = \frac{n}{2\Delta T}$.

For any practical purposes, a sampling rate of at least 4 or even 10 times the critical frequency is required in order to deal with phenomena such as aliasing and response spectrum shocks. For time-limited signals, thus, assuming that the energy of the signal in the time domain is bounded i.e., $\|f_\infty\|_{L^1} < C_f$, then for all practical purposes, the critical frequency ν_c can be set as the frequency beyond which the amplitude of the Fourier transform can be considered negligible, i.e., lower than a certain threshold, say $\epsilon_\nu \ll 1$.

A continuation method for Newton's iterations. For Newton-type schemes, the speed of the convergence to (or the divergence from) the solution depends on the choice of the initial guess, here for the unknown weights. Thus, we address a numerical natural continuation method for providing ‘‘good’’ initial guesses for the weights of the PIRPNN. Suppose that we have already converged to the solution in the interval $[t_{k-1} \quad t_k]$; we want to provide for the next time interval $[t_k \quad t_{k+1}]$, as computed from the proposed adaptation scheme described above, a good initial guess for the weights of the PIRPNN. We state the following proposition.

Proposition 2. Let $\Psi(t_k) \in \mathbb{R}^m$ be the solution found with PIRPNN at the end of the time interval $[t_{k-1} \quad t_k]$. Then, an initial guess for the weights of the PIRPNN for the time interval $[t_k \quad t_{k+1}]$ is given by:

$$\hat{W}^o = \frac{d\Psi(t_k)}{dt} \frac{\Phi^T}{\|\Phi\|_{l_2}^2}, \quad (30)$$

where $\hat{W}^o \in \mathbb{R}^{m \times N}$ is the matrix with the initial guess of the output weights of the m PIRPNNs and $\Phi \in \mathbb{R}^N$ is the vector containing the values of the random basis functions in the interval $[t_k \quad t_{k+1}]$.

Proof. At time t_k , a first-order estimation of the solution $\Psi(t_{k+1}) \in \mathbb{R}^m$ is given by:

$$\hat{\Psi}(t_{k+1}) = \Psi(t_k) + \frac{d\Psi(t_k)}{dt} (t_{k+1} - t_k), \quad (31)$$

where $\frac{d\Psi(t_k)}{dt}$ is known. For the next time interval $[t_k \quad t_{k+1}]$, the approximation of the solution with the PIRPNNs reads:

$$\Psi(t_{k+1}) = \Psi(t_k) + (t_{k+1} - t_k) \mathbf{W}^o \Phi. \quad (32)$$

By Eqs.(31), (32), we get:

$$\hat{W}^o \Phi = \frac{d\Psi(t_k)}{dt}. \quad (33)$$

It can be easily seen, that the economy SVD decomposition of the N -dimensional vector Φ is given by:

$$\Phi_{N \times 1} = \mathbf{U}_{N \times 1} \sigma_1, \quad \mathbf{U}_{N \times 1} = \frac{\Phi_{N \times 1}}{\|\Phi\|_{l_2}}, \quad \sigma_1 = \|\Phi\|_{l_2}. \quad (34)$$

Thus, the pseudo-inverse of Φ , is $\Phi^\dagger = \frac{\Phi^T}{\|\Phi\|_{l_2}^2}$. Hence, by Eq.(33), an initial guess for the weights for the time interval $[t_k \quad t_{k+1}]$ is given by:

$$\hat{W}^o = \frac{d\Psi(t_k)}{dt} \Phi^\dagger = \frac{d\Psi(t_k)}{dt} \frac{\Phi^T}{\|\Phi\|_{l_2}^2}. \quad (35)$$

□

Estimation of the interval of uniform distribution based on the variance/bias trade-off decomposition Based on the choice of Gaussian basis functions, from Eqs.(6), (13) one has to choose the number N of the basis functions, and the interval of the uniform distribution say $\mathcal{U} = [0 \ \alpha_{max}]$, from which the values of the shape parameters α_i are drawn. The theorems of uniform convergence (sections 2.3 and 2.4.1) consider the problem from the function approximation point of view. Regarding the approximation of a discrete set of data points, it has been proved that a set of N randomly and independently constructed vectors in the hypercube $[0, 1]^n$ will be pair-wise ϵ -orthogonal (i.e., $|\phi_i^T \phi_j| < \epsilon, \forall i, j, i \neq j$) with probability $1 - \theta$, where θ is sufficiently small for $N < \exp(\epsilon^2 n/4)\sqrt{\theta}$ [30].

Here, we construct N random vectors by parsimoniously sampling the values of the shape parameter from an appropriately bounded uniform interval for minimizing the two sources of error approximation, i.e., the bias and the variance in order to get good generalization properties. In our scheme, these, over all possible values of the shape parameter α are given by (see Eq.(19)):

$$\begin{aligned} \mathcal{B} &= \mathbb{E} \left[\sum_{j=1}^N w_j^o e^{-\alpha_j(t-t_j)^2} \right] - I_n(t), \\ \text{Var} &= \mathbb{E} \left[\left(\sum_{j=1}^N w_j^o e^{-\alpha_j(t-t_j)^2} \right)^2 \right] - \mathbb{E} \left[\sum_{j=1}^N w_j^o e^{-\alpha_j(t-t_j)^2} \right]^2, \end{aligned} \quad (36)$$

where \mathbb{E} denotes expectation operator. Overfitting, i.e., a high variance occurs for large values of α and underfitting, i.e., a high bias occurs for small values of α .

The expected value of the kernel $\phi(t - t_j; \alpha) = e^{-\alpha(t-t_j)^2}$, $t \neq t_j$ with respect to the probability density function of the uniform distribution of the random variable α reads:

$$\mathbb{E}[\phi(t - t_j; \alpha)] = \int_0^{\alpha_{max}} f_\alpha(\alpha) e^{-\alpha(t-t_j)^2} d\alpha = \frac{1 - e^{-\alpha_{max}(t-t_j)^2}}{\alpha_{max}(t-t_j)^2}. \quad (37)$$

Similarly, the variance is given by:

$$\begin{aligned} \text{Var}[\phi(t - t_j; \alpha)] &= \int_0^1 \phi^2 \frac{1}{\alpha_{max}(t-t_j)^2} \frac{1}{\phi} d\phi - \mathbb{E}[\phi]^2 = \\ &= \frac{1 - e^{-2\alpha_{max}(t-t_j)^2}}{2\alpha_{max}(t-t_j)^2} - \mathbb{E}[\phi]^2. \end{aligned} \quad (38)$$

At the limits of $t - t_j = dt = \frac{t_{end} - t_0}{N}$, from Eqs.(37),(38), we get:

$$\begin{aligned} \mathbb{E}[\phi(dt; \alpha)] &= \frac{N^2}{(t_{end} - t_0)^2} \frac{1 - e^{-\alpha_{max} \frac{(t_{end} - t_0)^2}{N^2}}}{\alpha_{max}}, \\ \text{Var}[\phi(dt; \alpha)] &= \frac{N^2}{(t_{end} - t_0)^2} \frac{1 - e^{-2\alpha_{max} \frac{(t_{end} - t_0)^2}{N^2}}}{2\alpha_{max}} - \mathbb{E}[\phi(dt; \alpha)]^2, \end{aligned} \quad (39)$$

The above expressions suggest that $\alpha_{max} = \frac{N^2}{c^2(N) (t_{end} - t_0)^2}$, $c(N) > 0$. This leaves us with only one parameter $c = c(N)$ to be determined for the ‘‘optimal’’ estimation of the upper bound of the uniform interval. Here, the value of $c(N)$ is found based on a reference solution, say \mathbf{u}_{ref} resulting from the integration of a stiff problem, which solution profiles contain also sharp gradients. For our computations, we have chosen as reference solution the one resulting from the van der Pol (vdP) ODEs given by:

$$\frac{du_1}{dt} = u_2, \quad \frac{du_2}{dt} = \mu(1 - u_1^2)u_2 - u_1, \quad (40)$$

for $\mu = 100$ and $u_1(0) = 2$, $u_2(0) = 0$ as initial conditions; the time interval was set to $[0 \ 3\mu]$, i.e., approximately three times the period of the relaxation oscillations, which for $\mu \gg 1$, is $T \approx \mu(3 - 2 \ln 2)$. The particular choice of $\mu = 100$ results to a stiff problem, thus containing very sharp gradients resembling approximately a discontinuity

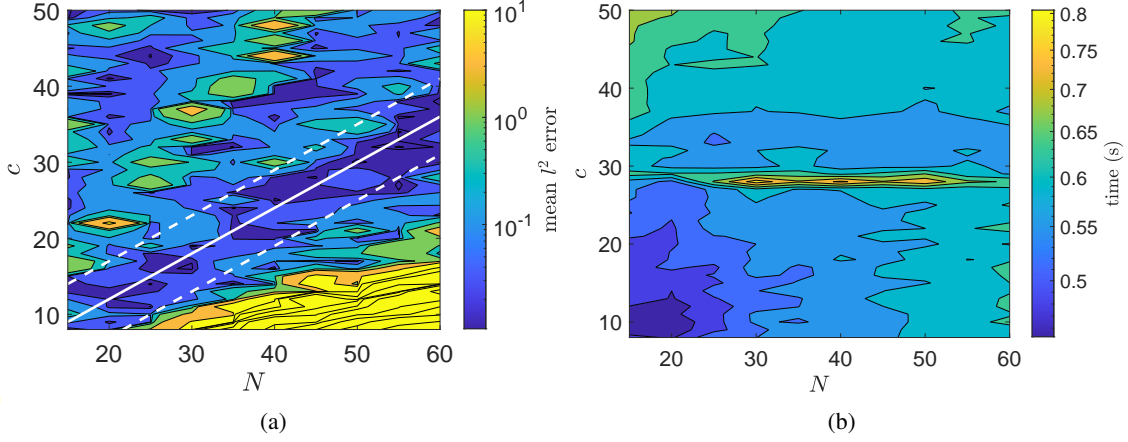


Figure 1: The numerical solution of the van der Pol problem with the proposed PIRPNN with $\mu = 100$ in the interval $[0 \quad 3\mu]$ with respect to c and N for $n = 20$; $RelTol$ and $AbsTol$ were set to $1e-06$; (a) Sum of the Bias and Variance of the approximation with respect to the reference solution as obtained with `ode15s` with $AbsTol$ and $RelTol$ set at $1e-14$, (b) Computational Times (s).

in the solution profile within the integration interval. The reference solution was obtained using the `ode15s` of the MATLAB ODE suite with absolute and relative error tolerances equal to $1e-14$.

Here, in order to estimate the “optimal” values of c, N for the vdP problem, we computed the bias-variance loss function using 60,000 points in $[0 \quad 3\mu]$ fixing the number of collocation points to $n = 20$. In Figure 1, we show the contour plots of the bias and variance errors and the computational times required for convergence, with both absolute tolerance and relative tolerance set to $1e-06$, for the vdP model. As can be seen in Figure 1(a) there is a linear band of “optimal” combinations of c, N within which the bias-variance error is for any practical purposes the same of the order of $\sim 1e-2$. In particular, this band can be coarsely described by a linear relation of the form $c \approx \frac{2}{5}N, N \geq 20$. Furthermore, as shown in Figure 1(b), within this band of “optimal” combinations, the computational cost is minimum for $c \sim 12, N = n = 20$. Based on the above, the parsimonious of the variables N and c are $N = 20, c = 12$ giving the best numerical accuracy and minimum computational cost. We note that the above parsimonious optimal values are set fixed once and for all for all the benchmark problems that we consider here.

2.4.4 The algorithm

We summarize the proposed method in the pseudo-code shown in Algorithm 1, where $\mathcal{U}(a, b)$ denotes the uniform random distribution in the interval (a, b) and $FlagSparse$ is a logic variable for choosing either the SVD or the sparse QR factorization.

3 Numerical Results

We implemented the proposed algorithm 1 using MATLAB 2020b on an Intel Core i7-10750H CPU @ 2.60GHz with up to 3.9 GHz frequency and a memory of 16 GBs. In all our computations, we have used a fixed number of collocation points $n = 20$ and number of basis functions $N = 20$ with $c = 12$ as discussed above. The Moore-Penrose pseudoinverse of $\nabla_{w^o} F$ was computed with the MATLAB built-in function `pinv`, with the default tolerance.

As stated, for assessing the performance of the proposed scheme, we considered seven benchmark problems of stiff ODEs and index-1 DAEs. In particular, we considered four index-1 DAEs, namely, the Robertson [60, 66] model of chemical kinetics, a problem of mechanics [66], a power discharge control problem [66], the index-1 DAE chemical Akzo Nobel problem [51, 72], and three stiff systems of ODEs, namely, the Belousov-Zhabotinsky chemical model [7, 77], the Allen-Chan metastable PDE phase-field model [2, 73] and the Kuramoto-Sivashinsky PDE [70, 73]. For comparison purposes, we used three solvers of the MATLAB ODE suite [65], namely `ode15s` and `ode23t` for DAEs and also `ode23s` for stiff ODEs, thus using the analytical Jacobian. In order to estimate the numerical approximation error, we used as reference solution the one computed with `ode15s` setting the absolute and relative error tolerances to $1e-14$. To this aim, we computed the l^2 and l^∞ norms of the differences between the computed and the reference solutions, as well as the mean absolute error (MAE). Finally, we ran each solver 10 times and computed the median, maximum and minimum computational times. For the PIRPNN the reported accuracy is the mean value of 10 es-

Algorithm 1 Solving IVPs of ODEs and index-1 DAEs using PIRPNNs

Require: $M \frac{du}{dx} = \mathbf{f}(t, \mathbf{u})$ in $[0 \ t_{end}]$ ▷ The ODE/ DAE system

Require: $u_i(0) = z_i$, for $i = 1, 2, \dots, m$ ▷ Set/Find Consistent Initial conditions

Require: Abstol, RelTol, FlagSparse ▷ Set # Neurons and # Collocation Points

1: $N \leftarrow 20$; $n \leftarrow 20$; ▷ Initialization of Derivatives

2: $Der_i = 0$; ▷ Set max # iters for Newton's iterations

3: $\nu_{max} \leftarrow 5$; ▷ set initial interval, see [28, 32]

4: $t^* \leftarrow 0$; $\Delta t \leftarrow \text{set_step_size}(\mathbf{f}, \mathbf{z}, \text{AbsTol}, \text{RelTol})$;

5: **repeat**

6: Select $t_l \in [t^* \ t^* + \Delta t]$; $l = 1, \dots, n$ ▷ Set # Collocation Points

7: $c_j \leftarrow t^* + j \frac{\Delta t}{N-1}$; $j = 1, \dots, N$ ▷ Set the Centers of Gaussian kernels

8: $\alpha_{ji} \sim \mathcal{U}\left(0, \frac{25}{9\Delta t^2}\right)$; ▷ Uniformly Distributed Shape Parameters of Gaussian kernels

9: $\mathbf{w}_i^o = Der_i \cdot \frac{\Phi^T}{\|\Phi\|_2^2}$; ▷ Natural Continuation for an Initial Guess (see Eq.(30))

10: $\mathcal{N}_i(t, \mathbf{w}_i^o, \mathbf{p}_i) \leftarrow \sum_{j=1}^N w_{ji}^o \exp(-\alpha_{ji}(t - c_j)^2)$ ▷ Construct the RPNN

11: $\Psi_{N_i}(t, \mathbf{w}_i^o) = z_i + (t - t^*)\mathcal{N}_i(t, \mathbf{w}_i^o, \mathbf{p}_i)$ ▷ (see Eqs.(16),(23) and (23))

12: $\nu \leftarrow 0$; ▷ Counter for Newton Iterations

13: **repeat**

14: **for** $l = 1, \dots, n$ and $i = 1, \dots, m$ **do**

15: $q \leftarrow l + (i-1)n$ ▷ Construct Residuals (see Eq.(24))

16: $F_q(\mathbf{W}^o) \leftarrow \sum_{j=1}^m M_{ij} \frac{d\Psi_{N_j}}{dt_i}(t_l, \mathbf{w}_j^o) - f_i(t_l, \Psi_{N_1}(t_l, \mathbf{w}_1^o), \dots, \Psi_{N_m}(t_l, \mathbf{w}_m^o))$;

17: **end for**

18: Set $\mathbf{F}(\mathbf{W}^o) = [F_1(\mathbf{W}^o), F_2(\mathbf{W}^o), \dots, F_{(nm)}(\mathbf{W}^o)]^T$

19: **if** $\nu \leq 1$ **then** ▷ Apply Quasi-Newton scheme

20: $J \leftarrow \nabla_{\mathbf{W}^o} \mathbf{F}(\mathbf{W}^o)$ ▷ Compute Jacobian Matrix

21: **if** FlagSparse is 'False' **then**

22: $J^\dagger \leftarrow V_\epsilon \Sigma_\epsilon^\dagger U_\epsilon^T$ ▷ Compute Pseudo-Inverse with SVD

23: **end if**

24: **end if**

25: **if** FlagSparse is 'False' **then**

26: $d\mathbf{W}^o \leftarrow -J^\dagger \mathbf{F}(\mathbf{W}^o)$;

27: **else**

28: $d\mathbf{W}^o \leftarrow \text{spqr_solve}(J, -\mathbf{F}, 'solution', 'min2norm')$; ▷ SuiteSparseQR [18, 19]

29: **end if**

30: $\mathbf{W}^o \leftarrow \mathbf{W}^o + d\mathbf{W}^o$;

31: $err \leftarrow \left\| \frac{\mathbf{F}(\mathbf{W}^{o(\nu)})}{\text{AbsTol} + \text{RelTol} \cdot \frac{d\Psi^{(k)}}{dt}} \right\|_{l^2}$; ▷ Compute Approximation Error (28)

32: $\nu \leftarrow \nu + 1$;

33: **until** ($err < 1$) or ($\nu \geq \nu_{max}$)

34: **if** $err < 1$ **then**

35: $t^* \leftarrow t^* + \Delta t$;

36: $Der_i = \frac{d\Psi_{N_i}(t^*)}{dt}$; ▷ Derivative at End Point

37: **end if**

38: $\Delta t \leftarrow 0.8 \cdot \min\left(0.1, \max\left(4, \frac{1}{err^{\frac{1}{\nu+1}}}\right)\right) \cdot \Delta t$; ▷ Adapt Step Size (29)

39: **until** $t^* = t_{end}$

timates. The initial time interval was selected according to the code in Chapter II.4 in [32] (for further details see [28]).

3.1 Case Study 1: The Robertson index-1 DAEs

The Robertson model describes the kinetics of an autocatalytic reaction [60]. This system of three DAEs is part of the benchmark problems considered in [66]. The set of the reactions reads:



where A, B, C are chemical species and $k_1 = 0.04, k_2 = 10^4$ and $k_3 = 3 \times 10^7$ are reaction rate constants. Assuming that the total mass of the system is conserved, we have the following system of index-1 DAEs:

$$\begin{aligned} \frac{dA}{dt} &= -k_1 A + k_2 BC, \\ \frac{dB}{dt} &= +k_1 A - k_2 BC - k_3 B^2, \\ A + B + C &= 1, \end{aligned} \tag{42}$$

where A, B and C denote the concentrations of $[A], [B]$ and $[C]$, respectively. In our simulations, we set $A(0) = 1, B(0) = 0$ as initial conditions of the concentrations and a very large time interval $[0 \quad 4 \cdot 10^{11}]$ as proposed in [54]. Table 1 summarizes the l^2, l^∞ and mean absolute (MAE) approximation errors with respect to the reference solution

Table 1: The Robertson index-1 DAEs (42) [66] in the time interval $[0 \quad 4 \cdot 10^{11}]$. l^2, l^∞ and mean absolute (MAE) approximation errors obtained with both absolute and relative tolerances set to $1e-03$ and $1e-06$.

		$tol = 1e-03$			$tol = 1e-06$		
		l^2	l^∞	MAE	l^2	l^∞	MAE
A	PIRPNN	2.08e-01	1.37e-02	2.47e-04	2.07e-04	6.69e-06	4.29e-07
	ode23t	Inf	Inf	Inf	3.41e+00	2.13e-01	3.10e-03
	ode15s	3.85e+09	1.92e+08	3.86e+06	2.84e+09	1.62e+08	2.15e+06
B	PIRPNN	1.79e-06	1.33e-07	1.79e-09	9.86e-10	5.48e-11	2.02e-12
	ode23t	Inf	Inf	Inf	3.41e+00	2.13e-01	3.10e-03
	ode15s	4.57e-03	2.42e-04	4.81e-06	1.56e-04	4.00e-06	1.75e-07
C	PIRPNN	2.08e-01	1.37e-02	2.47e-04	2.07e-04	6.69e-06	4.29e-07
	ode23t	Inf	Inf	Inf	1.10e-03	1.75e-05	2.92e-06
	ode15s	3.85e+09	1.92e+08	3.86e+06	2.84e+09	1.62e+08	2.15e+06

in 40,000 logarithmically spaced grid points in the interval $[0 \quad 4 \cdot 10^{11}]$. As shown, for the given tolerances, the proposed method outperforms ode15s and ode23t in all metrics. As it is shown in Figure 2, for tolerances $1e-03$, the proposed scheme achieves more accurate solutions than ode23t and ode15s. Actually, as shown, for the given tolerances, both ode23t and ode15s fail to approximate the solution up to the final time. In Table 3.1, we report the

Table 2: The Robertson index-1 DAEs (42). Computational times (s) (median, minimum and maximum over 10 runs) and number of points required in the interval $[0 \quad 4 \cdot 10^{11}]$ by the PIRPNN, ode23t and ode15s with both absolute and relative tolerances set to $1e-03$ and $1e-06$.

	$tol = 1e-03$				$tol = 1e-06$			
	median	min	max	# pts	median	min	max	# pts
PIRPNN	2.66e-02	2.32e-02	3.97e-02	640	3.47e-02	3.15e-02	4.11e-02	682
ode23t	7.09e-03	6.74e-03	1.16e-02	199	1.42e-02	1.38e-02	1.64e-02	613
ode15s	1.02e-02	9.69e-03	1.84e-02	271	2.11e-02	2.00e-02	2.18e-02	696
reference	1.15e-01	1.12e-01	1.22e-01	5194	1.15e-01	1.12e-01	1.22e-01	5194

computational times and number of points required by each method, including the time for computing the reference solution. As shown, the corresponding total number of points required by the proposed scheme is comparable with the ones required by ode23t and ode15s and significantly less than the number of points required by the reference solution. Furthermore, the computational times of the proposed method are comparable with the ones required by the ode23t and ode15s, thus outperforming the ones required for computing the reference solution.

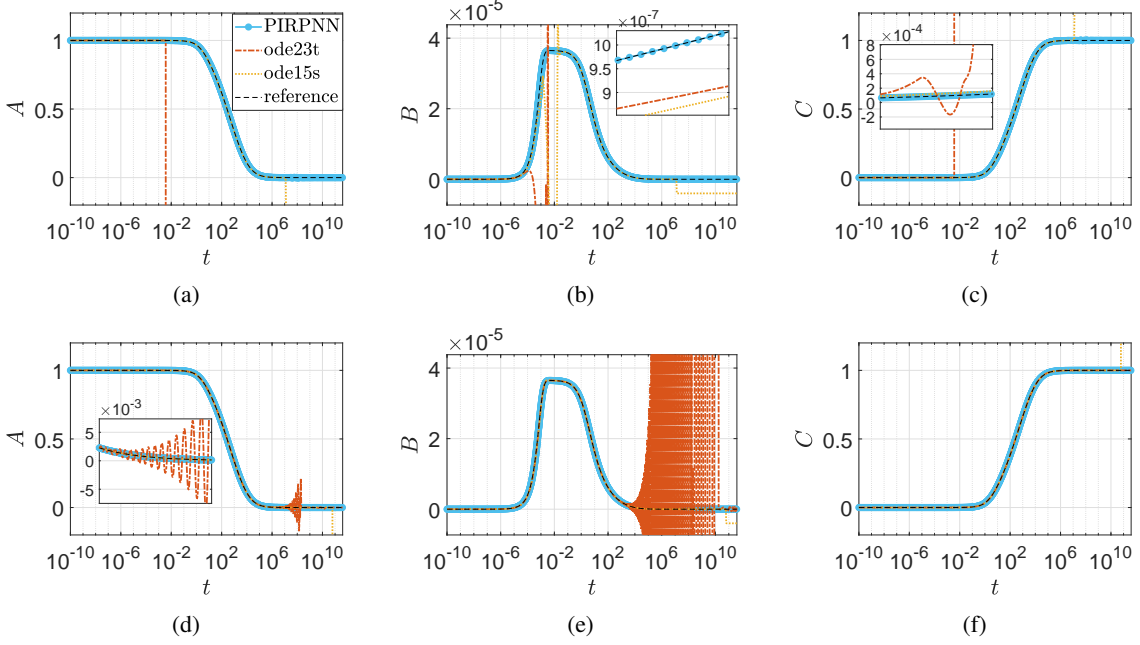


Figure 2: The Robertson index-1 DAEs (42) [66]. Approximate solutions computed in the interval $[0 \quad 4 \cdot 10^{11}]$ with both absolute and relative tolerances set to $1e-03$ ((a), (b) and (c)) and $1e-06$ ((d), (e) and (f)). Insets depict zooms around the reference solution.

3.2 Case Study 2: a mechanics non autonomous index-1 DAEs model

This is a non autonomous system of five index-1 DAEs and it is part of the benchmark problems considered in [66]. It describes the motion of a bead on a rotating needle subject to the forces of gravity, friction, and centrifugal force. The equations of motion are:

$$\begin{aligned}
\frac{du_1}{dt} &= u_2, \\
\frac{du_2}{dt} &= -10u_2 + \sin(t + \pi/4)u_5, \\
\frac{du_3}{dt} &= u_4, \\
\frac{du_4}{dt} &= -10u_4 - \cos(t + \pi/4)u_5 + 1, \\
0 &= g_{pp} + 20g_p + 100g,
\end{aligned} \tag{43}$$

where

$$\begin{aligned}
g &= \cos(t + \pi/4)u_3 - \sin(t + \pi/4)u_1, \\
g_p &= \cos(t + \pi/4)(u_4 - u_1) + \sin(t + \pi/4)(-u_2 - 2 - u_3), \\
g_{pp} &= \cos(t + \pi/4)\left(\frac{du_4}{dt} - \frac{du_1}{dt} - u_2 - u_3 + \sin(t + \pi/4)\left(-\frac{du_2}{dt} - \frac{du_3}{dt} - u_4 + u_1\right)\right).
\end{aligned} \tag{44}$$

The initial conditions are $u_1(0) = 1$, $u_2(0) = -6$, $u_3(0) = 1$, $u_4(0) = -6$ and a consistent initial condition for $u_5(0) = -10.60660171779820$ was found with Newton-Raphson at $t = 0$, with a tolerance of $1e-16$. Table 3 summarizes the l^2 , l^∞ and mean absolute (MAE) errors with respect to the reference solution in 15,000 equally spaced grid points in the interval $[0 \quad 15]$. As shown, for the given tolerances, the proposed method outperforms ode15s and ode23t in all metrics. As it is shown in Figure 3, for tolerances $1e-03$, the proposed scheme achieves more accurate solutions than ode23t and ode15s. In Table 3.2, we report the computational times and number of points required by each method, including the ones required for computing the reference solution. As shown, the corresponding total number of points required by the proposed scheme is comparable with the ones required by ode15s and significantly less than the number of points required by ode23t and the reference solution. Furthermore, the computational times of the proposed method are comparable with the ones required by the ode23t and 15s, thus outperforming the ones required for computing the reference solution.

Table 3: The mechanics problem of non autonomous index-1 DAEs (43) in $[0, 15]$. l^2 , l^∞ and mean absolute (MAE) approximation errors obtained with both absolute and relative tolerances set to $1e-03$ and $1e-06$.

		$tol = 1e-03$			$tol = 1e-06$		
		l^2	l^∞	MAE	l^2	l^∞	MAE
u_1	PIRPNN	3.64e-05	7.77e-07	2.06e-07	9.70e-07	2.57e-08	4.71e-09
	ode23t	6.26e-01	1.69e-02	3.34e-03	8.41e-03	2.19e-04	4.56e-05
	ode15s	6.38e-01	1.90e-02	3.12e-03	3.59e-04	8.89e-06	1.96e-06
u_2	PIRPNN	4.95e-05	1.42e-06	2.55e-07	3.08e-06	1.49e-07	1.22e-08
	ode23t	4.38e-01	1.04e-02	2.25e-03	6.18e-03	1.35e-04	3.23e-05
	ode15s	6.57e-01	1.49e-02	3.60e-03	2.94e-04	1.40e-05	1.59e-06
u_3	PIRPNN	3.78e-05	8.05e-07	2.12e-07	9.90e-07	3.06e-08	4.78e-09
	ode23t	5.79e-01	1.27e-02	3.15e-03	7.88e-03	1.68e-04	4.36e-05
	ode15s	5.72e-01	1.22e-02	2.91e-03	3.02e-04	7.36e-06	1.58e-06
u_4	PIRPNN	5.13e-05	1.93e-06	2.49e-07	2.98e-06	1.34e-07	1.18e-08
	ode23t	4.50e-01	1.35e-02	2.30e-03	6.42e-03	1.82e-04	3.27e-05
	ode15s	6.89e-01	2.03e-02	3.53e-03	3.87e-04	2.38e-05	1.86e-06
u_5	PIRPNN	7.53e-04	3.12e-05	4.11e-06	4.63e-05	2.00e-06	2.01e-07
	ode23t	6.39e+00	1.39e-01	3.53e-02	9.00e-02	1.95e-03	5.05e-04
	ode15s	9.61e+00	2.04e-01	5.65e-02	4.56e-03	1.10e-04	2.60e-05

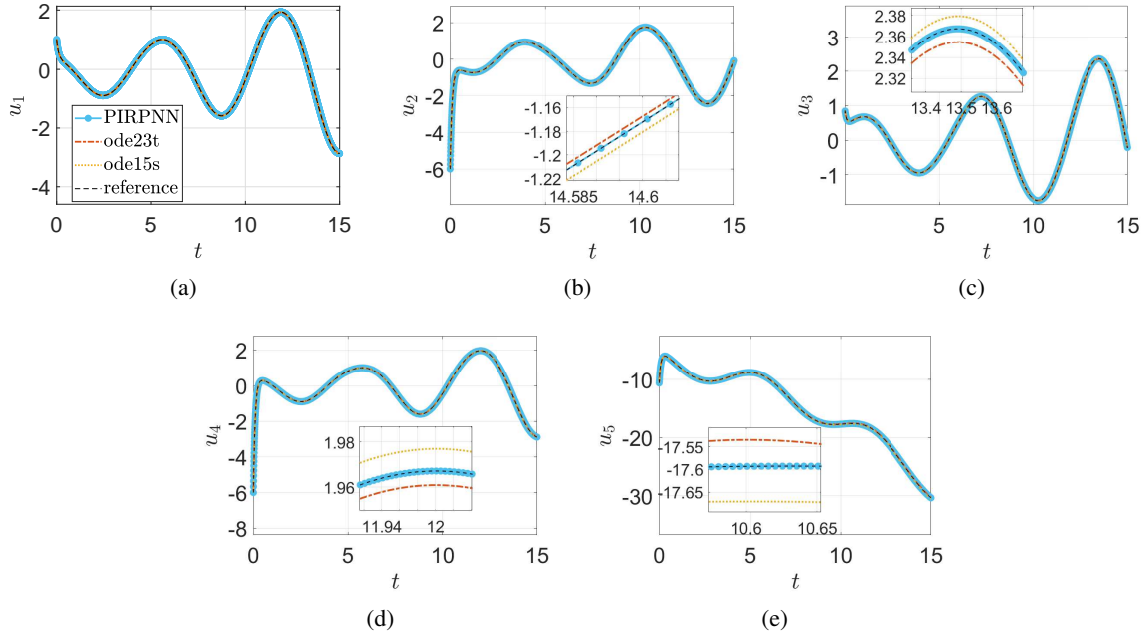


Figure 3: The mechanics problem of non autonomous index-1 DAEs (43) [66]. Approximate solutions computed in the interval $[0, 15]$ with both absolute and relative tolerances set to $1e-03$. Insets depict zooms around the reference solution.

Table 4: The mechanics problem of non autonomous index-1 DAEs [66] (43). Computational times (s) (median, minimum and maximum over 10 runs) and number of points required in the interval [0 15] by the PIRPNN, ode23t and ode15s with both absolute and relative tolerances set to 1e−03 and 1e−06.

	tol = 1e−03				tol = 1e−06			
	median	min	max	# pts	median	min	max	# pts
PIRPNN	1.72e−02	1.38e−02	3.09e−02	140	2.33e−02	1.96e−02	2.63e−02	200
ode23t	4.97e−03	4.66e−03	3.23e−02	157	1.81e−02	1.72e−02	3.87e−02	1320
ode15s	4.71e−03	4.45e−03	1.08e−02	145	7.75e−03	7.57e−03	1.51e−02	295
reference	3.18e−01	3.06e−01	4.92e−01	20734	3.17e−01	3.05e−01	4.92e−01	20734

3.3 Case Study 3: Power discharge control non autonomous index-1 DAEs model

This is a non autonomous model of six index-1 DAEs and it is part of the benchmark problems considered in [66]. The governing equations are:

$$\begin{aligned}
 \frac{du_1}{dt} &= \frac{(u_2 - u_1)}{20}, \\
 \frac{du_2}{dt} &= -\frac{(u_4 - 99.1)}{75}, \\
 \frac{du_3}{dt} &= \mu - u_6, \\
 0 &= 20u_5 - u_3 \\
 0 &= (3.35 - 0.075u_6 + 0.001u_6^2) - \frac{u_4}{u_5}, \\
 0 &= \frac{u_3}{400} \frac{du_3}{dt} + \frac{\mu\mu_p}{(1.2u_1)^2} - \frac{du_1}{dt} \frac{\mu^2}{(1.44u_1)^3}, \\
 \mu &= 15 + 5\tanh(t - 10), \quad \mu_p = \frac{5}{\cosh^2(t - 10)}.
 \end{aligned} \tag{45}$$

The initial conditions are $u_1(0) = u_2(0) = 0.25$, $u_3(0) = 734$, and consistent initial conditions for $u_4(0) = 99.08999492002$, $u_5(0) = 36.7$ and $u_6(0) = 10.00000251671$ were found at $t = 0$ with Newton-Raphson with a tolerance of 1e−16. Table 5 summarizes the l^2 , l^∞ and mean absolute (MAE) approximation errors with respect to

Table 5: Power discharge control non autonomous index-1 DAEs problem (45) in [0 40]. l^2 , l^∞ and mean absolute (MAE) approximation errors obtained with both absolute and relative tolerances set to 1e−03 and 1e−06.

		tol = 1e−03			tol = 1e−06		
		l^2	l^∞	MAE	l^2	l^∞	MAE
u_1	PIRPNN	1.37e−05	1.46e−07	5.59e−08	2.69e−06	2.27e−08	1.13e−08
	ode23t	1.98e−01	1.61e−03	8.40e−04	1.65e−03	1.21e−05	7.07e−06
	ode15s	1.83e−01	1.48e−03	7.96e−04	3.46e−04	2.32e−06	1.55e−06
u_2	PIRPNN	1.72e−04	3.27e−05	1.31e−07	4.49e−06	6.44e−08	1.96e−08
	ode23t	8.31e−01	1.04e−02	3.05e−03	2.47e−03	1.91e−05	1.10e−05
	ode15s	3.10e−01	2.80e−03	1.39e−03	5.45e−04	5.56e−06	2.47e−06
u_3	PIRPNN	1.02e−02	1.18e−04	3.96e−05	1.32e−04	9.95e−07	5.67e−07
	ode23t	9.36e+00	8.64e−02	3.74e−02	1.26e−01	1.21e−03	5.05e−04
	ode15s	7.05e+00	8.12e−02	2.78e−02	1.60e−02	1.50e−04	7.13e−05
u_4	PIRPNN	2.49e−03	4.87e−04	1.49e−06	1.96e−05	8.32e−07	6.50e−08
	ode23t	1.23e+01	1.56e−01	4.32e−02	1.15e−02	1.37e−04	4.57e−05
	ode15s	1.23e+00	2.17e−02	4.02e−03	4.42e−03	4.93e−05	1.91e−05
u_5	PIRPNN	5.12e−04	5.88e−06	1.98e−06	6.60e−06	4.98e−08	2.83e−08
	ode23t	4.68e−01	4.32e−03	1.87e−03	6.28e−03	6.03e−05	2.52e−05
	ode15s	3.53e−01	4.06e−03	1.39e−03	8.00e−04	7.50e−06	3.57e−06
u_6	PIRPNN	1.36e−02	2.81e−03	5.58e−06	3.30e−05	5.35e−06	5.06e−08
	ode23t	8.07e+00	1.08e−01	2.84e−02	5.71e−02	8.05e−04	2.04e−04
	ode15s	1.31e+00	5.72e−02	3.54e−03	3.74e−03	1.32e−04	1.37e−05

the reference solution in 40,000 equally spaced grid points in the interval [0 40]. As shown, for the given tolerances,

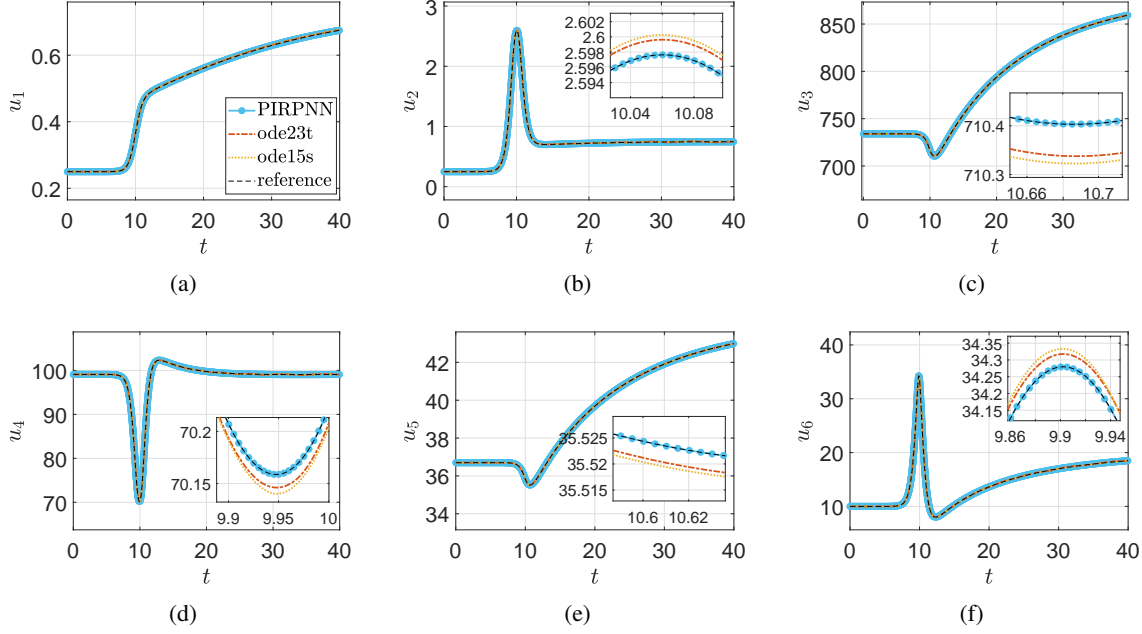


Figure 4: Power discharge control non autonomous index-1 DAEs problem (45) [66]. Approximate solutions computed in the interval $[0 \ 40]$ with both absolute and relative tolerances set to $1e-03$. Insets depict zooms around the reference solution.

the proposed method outperforms ode15s and ode23t in all metrics. As it is shown in Figure 4, for tolerances $1e-03$, the proposed scheme achieves more accurate solutions than ode23t and ode15s. In Table 3.3, we report the compu-

Table 6: Power discharge control non autonomous index-1 DAEs problem (45). Computational times (median, minimum and maximum over 10 runs) and number of points required in the interval $[0,40]$ by the PIRPNN, ode23t and ode15s with both absolute and relative tolerances set to $1e-03$ and $1e-06$.

	$tol = 1e-03$				$tol = 1e-06$			
	median	min	max	# pts	median	min	max	# pts
PIRPNN	8.55e-02	7.75e-02	9.93e-02	394	9.26e-02	8.65e-02	1.16e-01	470
ode23t	4.30e-03	2.65e-03	5.67e-02	69	1.06e-02	9.52e-03	4.97e-02	642
ode15s	2.93e-03	2.61e-03	1.49e-02	77	6.04e-03	5.68e-03	1.85e-02	229
reference	9.01e-02	8.88e-02	1.75e-01	5093	9.01e-02	8.88e-02	1.75e-01	5093

tational times and number of points required by each method, including the ones required for computing the reference solution. As shown, the corresponding total corresponding number of points required by the proposed scheme is comparable with the ones required by ode23t and ode15s and significantly less than the number of points required by the reference solution. Furthermore, the computational times of the proposed method are comparable with the ones required by the ode23t and ode15s, thus outperforming the ones required for computing the reference solution.

3.4 Case Study 4: The Chemical Akzo Nobel index-1 DAE model

The Chemical Akzo Nobel problem is a benchmark problem made up of six non-linear index-1 DAEs. This problem originates from Akzo Nobel research center in Amsterdam and was described in [51, 72]. The resulting system of

index-1 DAEs is given by:

$$\begin{aligned}
 \frac{du_1}{dt} &= -2k_1u_1^4u_2^{\frac{1}{2}} - \frac{k_2}{K}u_1u_5 + k_2u_3u_4 - k_3u_1u_4^2 \\
 \frac{du_2}{dt} &= -\frac{1}{2}k_1u_1^4u_2^{\frac{1}{2}} - k_3u_1u_4^2 - \frac{1}{2}k_4u_6^2u_2^{\frac{1}{2}} + k_{in}\left(\frac{\rho}{H} - u_2\right) \\
 \frac{du_3}{dt} &= k_1u_1^4u_2^{\frac{1}{2}} + \frac{k_2}{K}u_1u_5 - k_2u_3u_4 \\
 \frac{du_4}{dt} &= -\frac{k_2}{K}u_1u_5 + k_2u_3u_4 + k_4u_6^2u_2^{\frac{1}{2}} \\
 \frac{du_5}{dt} &= \frac{k_2}{K}u_1u_5 - k_2u_3u_4 - 2k_3u_1u_4^2 \\
 0 &= K_s u_1 u_4 - u_6,
 \end{aligned} \tag{46}$$

where u_1, u_2, \dots, u_6 denote the concentrations of 6 chemical species, $k_1 = 18.7$, $k_2 = 0.58$, $k_3 = 0.09$, $k_4 = 0.42$ and $K = 34.4$ are the reaction rate coefficients, $K_s = 115.83$ is a coefficient of proportionality between u_1u_4 and u_6 , and the constant injection of u_2 in the system is governed by a rate $k_{in} = 3.3$, and constants $\rho = 0.9$ and $H = 737$. The initial conditions are set as: $u_1 = 0.444$, $u_2 = 0.0012$, $u_3 = 0$, $u_4 = 0.007$, $u_5 = 0$.

Table 7: The chemical Akzo Nobel problem (46). Absolute error (l^2 -norm, l^∞ -norm and MAE) for the solutions computed with tolerances set to $1e-03$ and $1e-06$. The reference solution was obtained with ode15s with tolerances set to $1e-14$.

		$tol = 1e-03$			$tol = 1e-06$		
		l^2	l^∞	MAE	l^2	l^∞	MAE
u_1	PIRPNN	6.09e-04	3.84e-06	1.24e-06	1.35e-06	8.22e-09	2.42e-09
	ode23t	7.17e-02	5.90e-04	1.19e-04	1.88e-03	5.48e-06	4.29e-06
	ode15s	1.36e-01	1.21e-03	1.62e-04	2.87e-04	1.80e-06	6.11e-07
u_2	PIRPNN	8.66e-06	5.43e-07	7.98e-09	2.74e-08	7.97e-10	2.64e-11
	ode23t	8.24e-03	5.92e-05	1.74e-05	7.20e-06	5.41e-07	6.95e-09
	ode15s	1.33e-03	9.40e-05	9.48e-07	9.85e-06	9.88e-07	4.42e-09
u_3	PIRPNN	3.01e-04	1.92e-06	6.10e-07	6.55e-07	4.04e-09	1.17e-09
	ode23t	3.48e-02	2.86e-04	5.82e-05	9.38e-04	2.74e-06	2.14e-06
	ode15s	6.94e-02	6.15e-04	8.16e-05	1.44e-04	8.98e-07	3.07e-07
u_4	PIRPNN	1.13e-05	5.57e-08	2.14e-08	4.93e-08	4.96e-10	7.16e-11
	ode23t	2.93e-03	2.09e-05	3.93e-06	3.45e-05	2.40e-07	5.93e-08
	ode15s	3.62e-03	4.11e-05	4.50e-06	7.45e-06	4.90e-08	1.25e-08
u_5	PIRPNN	4.22e-04	1.54e-06	7.22e-07	3.26e-07	1.17e-09	6.48e-10
	ode23t	1.97e-02	5.51e-05	4.44e-05	3.04e-04	8.23e-07	6.86e-07
	ode15s	2.75e-02	9.01e-05	6.25e-05	4.61e-05	1.53e-07	1.03e-07
u_6	PIRPNN	2.59e-04	2.58e-06	5.09e-07	2.52e-06	4.25e-08	2.31e-09
	ode23s	1.42e-01	1.03e-03	2.54e-04	1.06e-03	7.97e-06	1.77e-06
	ode15s	8.30e-02	9.17e-04	1.06e-04	1.71e-04	1.42e-06	2.80e-07

Table 7 summarizes the approximation errors, in terms of l^2 -norm and l^∞ -norm errors and MAE, with respect to the reference solution in 180,000 equally spaced grid points in the interval $[0 \quad 180]$. As shown, for the given tolerances, the proposed method outperforms ode15s and ode23t in all metrics.

As it is shown in Figure 5, for tolerances $1e-03$, the proposed scheme achieves more accurate solutions than ode23t and ode15s. In Table 3.4, we report the number of points and the computational times required by each method, including the time for computing the reference solution. As shown, the corresponding total number of points required by the proposed scheme is comparable with the ones required by ode23t and 15s and significantly smaller than the number of points required by the reference solution. Furthermore, the computational times of the proposed method are comparable with the ones required by the ode23t and 15s, thus outperforming the ones required for computing the reference solution.

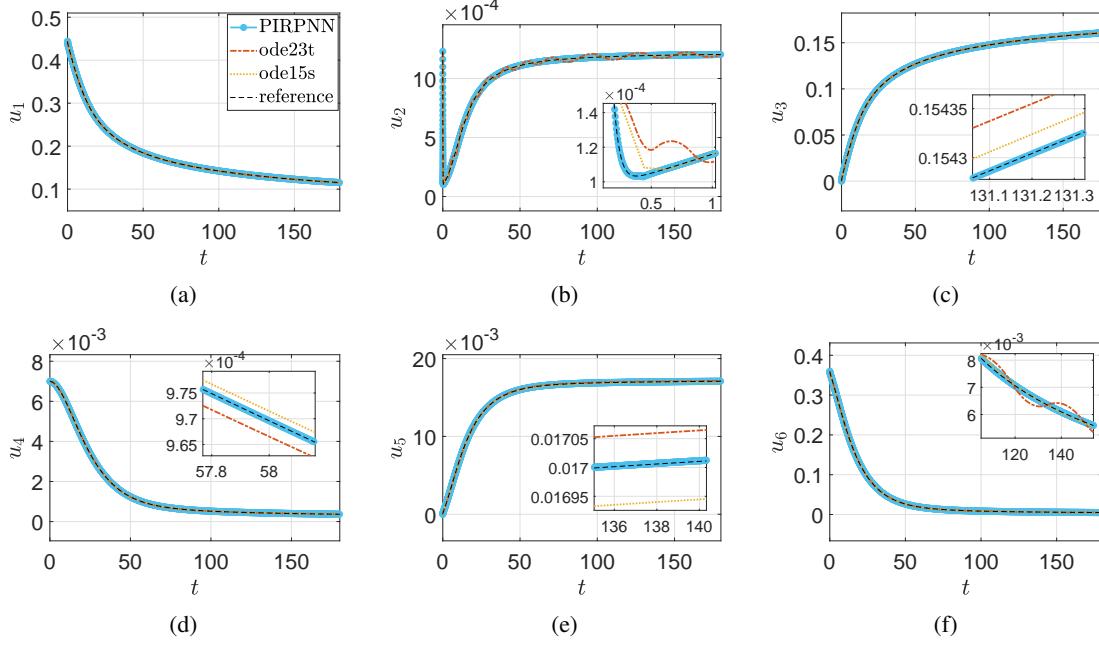


Figure 5: The chemical Akzo Nobel DAE problem (46). Approximate solutions computed in the interval $[0, 180]$ with both absolute and relative tolerances set to $1e-03$. Insets depict zooms around the reference solution.

Table 8: Chemical Akzo Nobel problem (46). Computational times in seconds (median, minimum and maximum over 10 runs) and Number of points required in the interval $[0, 180]$ by PIRPNN, ode23t and ode15s with tolerances $1e-03$ and $1e-06$. The reference solution was computed by ode15s with tolerances equal to $1e-14$.

	$tol = 1e-03$				$tol = 1e-06$			
	median	min	max	# pts	median	min	max	# pts
PIRPNN	2.90e-02	2.61e-02	4.82e-02	192	2.70e-02	2.58e-02	4.21e-02	204
ode23s	2.02e-03	1.90e-03	3.21e-03	31	6.28e-03	5.84e-03	2.23e-02	195
ode15s	3.54e-03	3.34e-03	3.73e-03	34	4.41e-03	4.17e-03	1.19e-02	107
reference	3.85e-02	3.71e-02	4.48e-02	1426	3.85e-02	3.71e-02	4.48e-02	3195

3.5 Case Study 5: The Belousov–Zhabotinsky stiff ODEs

The Belousov–Zhabotinsky chemical reactions model [8, 77] is given by the following system of seven ODEs:

$$\begin{aligned}
\frac{dA}{dt} &= -k_1AY, \\
\frac{dY}{dt} &= -k_1AY - k_2XY + k_5Z, \\
\frac{dX}{dt} &= k_1AY - k_2XY + k_3BX - 2k_4X^2, \\
\frac{dP}{dt} &= k_2XY, \\
\frac{dB}{dt} &= -k_3BX, \\
\frac{dZ}{dt} &= k_3BX - k_5Z, \\
\frac{dQ}{dt} &= k_4X^2.
\end{aligned} \tag{47}$$

A, B, P, Q, X, Y, Z are the concentrations of chemical species and $k_1 = 4.72$, $k_2 = 3 \times 10^9$, $k_3 = 1.5 \times 10^4$, $k_4 = 4 \times 10^7$, $k_5 = 1$ are the reaction coefficients. The initial conditions are set as $A(0) = B(0) = 0.066$,

$Y(0) = X(0) = P(0) = Q(0) = 0, Z(0) = 0.002$. This is a very stiff problem, due to the different scales of the reaction coefficients, thus exhibiting very sharp gradients. Indeed, for an acceptable solution is needed a tolerance at least of $1e-07$ as also reported in [67]. Here, we have compared the solution obtained with the proposed PIRPNN, with the stiff solvers ode23s and ode15s. Table 9 summarizes the l^2, l^∞ and mean absolute (MAE) approximation

Table 9: The Belousov–Zhabotinsky stiff ODEs problem (47) in the time interval $[0 \ 40]$. l^2, l^∞ and mean absolute (MAE) approximation errors obtained with both absolute and relative tolerances set to $1e-07$ and $1e-08$.

		$tol = 1e-07$			$tol = 1e-08$		
		l^2	l^∞	MAE	l^2	l^∞	MAE
A	PIRPNN	3.23e-04	5.87e-06	7.24e-07	6.92e-06	1.27e-07	1.54e-08
	ode23s	2.18e-02	4.40e-04	4.06e-05	2.44e-04	4.67e-06	6.28e-07
	ode15s	1.30e-01	1.37e-03	4.11e-04	8.29e-02	1.25e-03	1.69e-04
Y	PIRPNN	8.27e-04	4.09e-05	1.34e-06	1.78e-05	9.05e-07	2.86e-08
	ode23s	4.22e-02	1.19e-03	7.29e-05	6.69e-04	3.51e-05	1.14e-06
	ode15s	1.06e-01	1.31e-03	3.28e-04	5.88e-02	1.19e-03	1.12e-04
X	PIRPNN	4.77e-05	1.04e-05	1.29e-08	1.94e-06	9.43e-07	2.79e-10
	ode23s	2.60e-04	1.23e-05	1.87e-07	4.88e-05	1.16e-05	1.09e-08
	ode15s	3.21e-04	1.23e-05	2.71e-07	2.26e-04	1.23e-05	1.46e-07
P	PIRPNN	7.08e-04	4.15e-05	1.08e-06	1.53e-05	9.05e-07	2.32e-08
	ode23s	3.27e-02	8.16e-04	6.07e-05	5.54e-04	3.48e-05	9.69e-07
	ode15s	1.98e-01	2.03e-03	6.49e-04	1.35e-01	1.87e-03	2.95e-04
B	PIRPNN	2.99e-03	1.76e-04	1.83e-06	6.48e-05	3.86e-06	3.93e-08
	ode23s	1.09e-01	3.17e-03	1.09e-04	2.41e-03	1.49e-04	2.04e-06
	ode15s	4.05e-01	3.52e-03	1.25e-03	2.85e-01	3.18e-03	6.49e-04
Z	PIRPNN	2.73e-03	1.73e-04	2.93e-06	5.91e-05	3.84e-06	6.27e-08
	ode23s	7.85e-02	2.56e-03	1.12e-04	2.21e-03	1.48e-04	2.46e-06
	ode15s	1.24e-01	2.84e-03	2.55e-04	6.88e-02	2.56e-03	9.36e-05
Q	PIRPNN	1.26e-03	8.64e-05	7.36e-07	2.73e-05	1.92e-06	1.58e-08
	ode23s	4.38e-02	1.28e-03	4.34e-05	1.01e-03	7.36e-05	7.90e-07
	ode15s	1.64e-01	1.42e-03	5.03e-04	1.15e-01	1.28e-03	2.62e-04

errors with respect to the reference solution in 40,000 equally spaced grid points in the interval $[0 \ 40]$. As shown, for the given tolerances, the proposed method outperforms ode15s and ode23s in all metrics. As it is shown in Figure 6, for tolerances $1e-07$, the proposed scheme achieves more accurate solutions than ode23s and ode15s. Actually, as shown, for the given tolerances, both ode23s and ode15s fail to converge resulting in time shifted jumps, while also ode15s fails to approximate the solution up to the final time. In Table 3.5, we report the computational times

Table 10: Belousov-Zhabotinsky stiff ODEs problem (47). Computational times (s) (median, minimum and maximum over 10 runs) and number of points required in the interval $[0 \ 40]$ by the PIRPNN, ode23s and ode15s with both absolute and relative tolerances $1e-07$ and $1e-08$.

	$tol = 1e-07$				$tol = 1e-08$			
	median	min	max	# pts	median	min	max	# pts
PIRPNN	4.62e-01	4.13e-01	5.88e-01	1624	5.54e-01	4.98e-01	6.19e-01	2056
ode23s	1.04e-02	9.96e-03	1.57e-02	255	1.83e-02	1.77e-02	3.36e-02	480
ode15s	9.72e-03	9.44e-03	1.82e-02	251	1.37e-02	1.33e-02	2.52e-02	362
reference	8.79e-02	8.63e-02	1.59e-01	3195	8.79e-02	8.63e-02	1.59e-01	3195

and number of points required by each method, including the ones required for computing the reference solution. As shown, the corresponding total number of points required by the proposed scheme is larger than the ones required by ode23t and 15s (which however fail), but yet significantly less than the number of points required by the reference solution. Besides, the computational times required by the proposed method are for any practical purposes comparable with the ones required for computing the reference solution.

3.6 Case Study 6: The Allen-Cahn phase-field PDE

The Allen-Cahn equation is a famous reaction-diffusion PDE that was proposed in [2] as a phase-field model for describing the dynamics of the mean curvature flow. Here, for our illustrations, we considered a one-dimensional

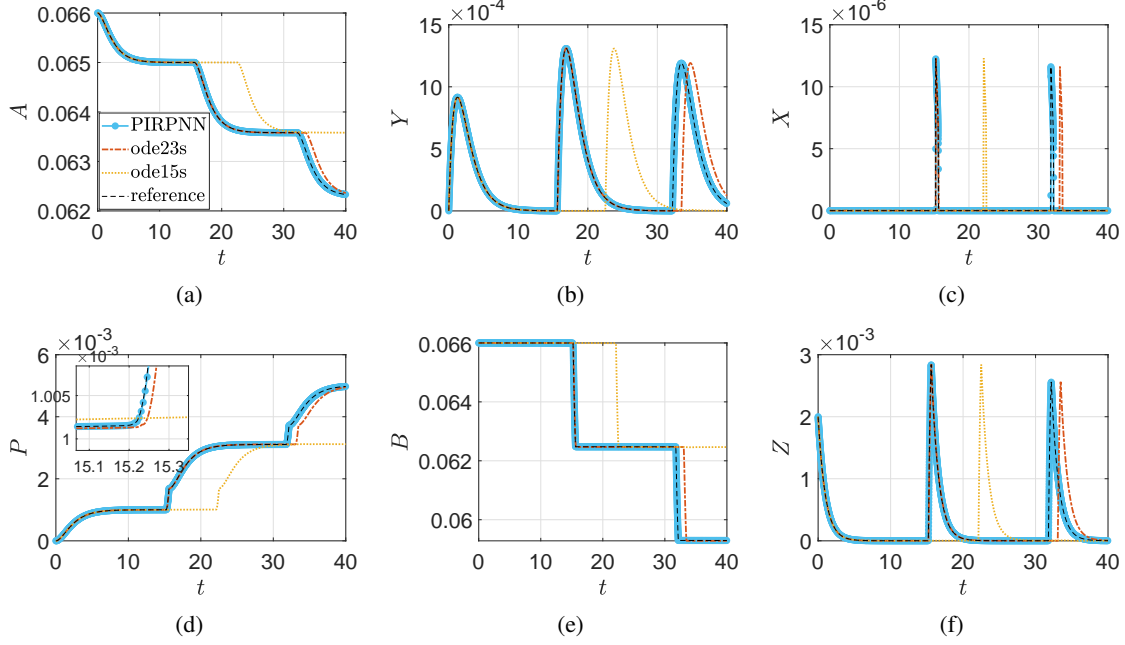


Figure 6: The Belousov–Zhabotinsky stiff ODEs problem (47) in the time interval $[0, 40]$. Approximate solutions of 6 chemical species (out of 7) computed by the PIRPNN, ode23s, ode15s with tolerances set to $1e-07$.

formulation given by [73]:

$$\frac{\partial u}{\partial t} = \nu \frac{\partial^2 u}{\partial x^2} + u - u^3, \quad x \in [-1, 1], \quad u(-1, t) = -1, \quad u(1, t) = 1, \quad (48)$$

with initial condition $u(x, 0) = 0.53x + 0.47 \sin(-1.5\pi x)$. For $\nu = 0.01$, the solution is stiff [73], thus exhibiting a metastable behavior with an initial two-hill configuration that disappears close to $t = 40$ with a fast transition to a one-hill stable solution. Here, we integrate this until $t = 70$. To solve the Allen-Cahn PDE, we used an equally spaced grid using (as in [73]) 102 points $x_0, x_1, \dots, x_{100}, x_{101}$ and second order centered finite differences. Hence, (48) becomes a system of 100 ODEs in $u_i(t) = u(x_i, t)$, $i = 1, \dots, 100$:

$$\frac{\partial u_i}{\partial t} = \nu \frac{(u_{i+1} - 2u_i + u_{i-1}))}{dx^2} + u_i - u_i^3, \quad u_0 = -1, \quad u_{101} = 1. \quad (49)$$

Here, for our computations, we have used a sparse QR decomposition as implemented in the SuiteSparseQR [18, 19]. Table 3.6 summarizes the l^2 , l^∞ and mean absolute (MAE) approximation errors with respect to the reference solution

Table 11: Allen-Cahn phase-field PDE (49) with $\nu = 0.01$ in $[0, 70]$. l^2 , l^∞ and mean absolute approximation (MAE) errors obtained with both absolute and relative tolerances set to $1e-03$ and $1e-06$.

	$tol = 1e-03$			$tol = 1e-06$		
	l^2	l^∞	MAE	l^2	l^∞	MAE
PIRPNN	6.36e-03	8.01e-05	2.19e-06	2.07e-05	1.43e-07	8.36e-09
ode23s	8.98e-01	1.12e-02	3.15e-04	2.46e-03	2.69e-05	1.16e-06
ode15s	3.74e+00	4.50e-02	1.17e-03	1.84e-03	2.33e-05	6.23e-07

in 7000×102 equally spaced grid points in the time interval $[0, 70]$ and in the space interval $[-1, 1]$, respectively. As shown, for the given tolerances, the proposed method outperforms ode15s and ode23s in all metrics. As it is shown in Figure 7, for tolerances $1e-03$, the proposed scheme achieves more accurate solutions than ode23s and ode15s. In Table 3.6, we report computational times and number of points required by each method, including the ones required for computing the reference solution. As shown, the corresponding total number of points required by the proposed scheme is comparable with the ones required by ode23s and ode15s and significantly less than the number of points required by the reference solution. On the other hand, the computing times of the proposed method are significantly larger than the ones required by ode23s and ode15s (Table 3.6) and also with the ones required by

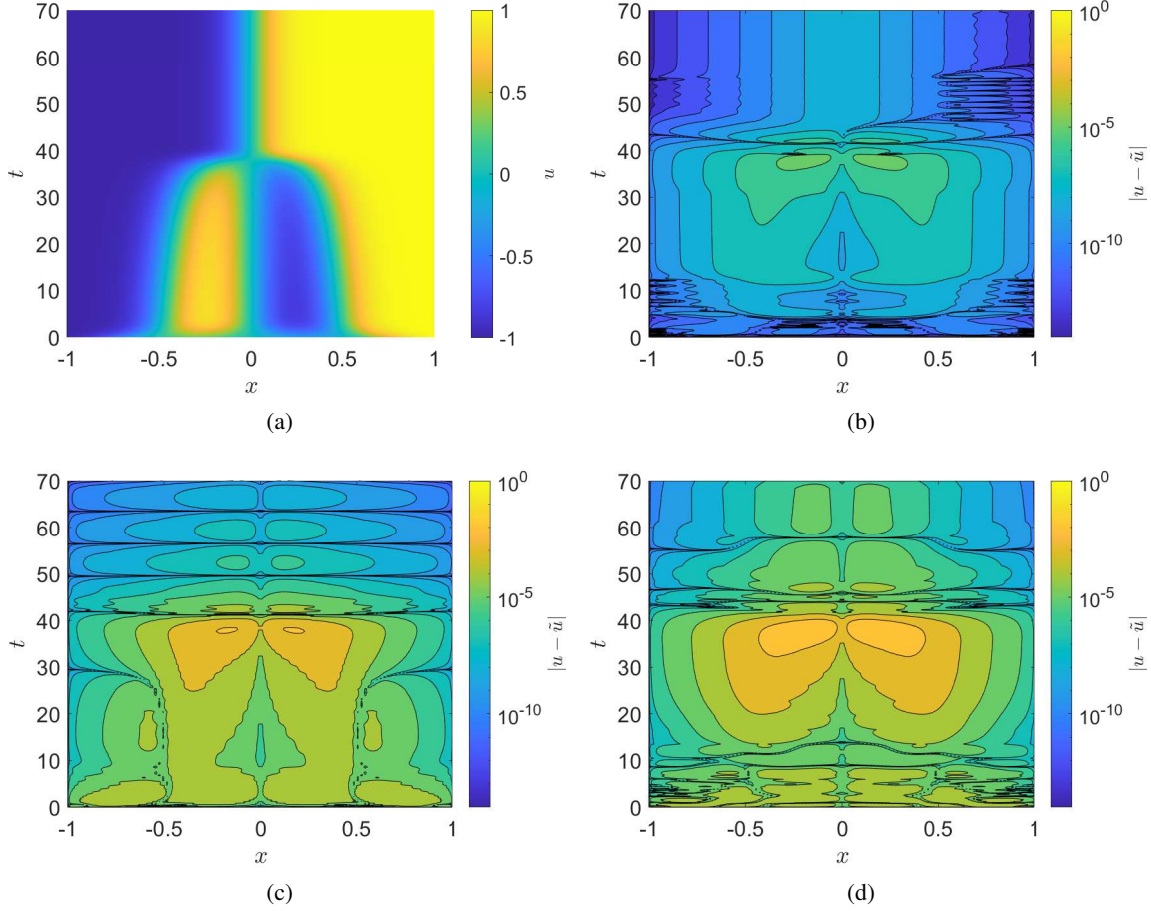


Figure 7: Allen-Cahn phase-field PDE discretized with FD (49) with $\nu = 0.01$ in the time interval $[0, 70]$. Contour plots of absolute point errors computed with tolerance $1e-03$: a) reference solution computed with ode15s with $\text{tol}=1e-14$, b) PIRPNN absolute errors c) ode23s absolute errors d) ode15s absolute errors.

Table 12: Allen-Cahn PDE phase-field PDE with $\nu = 0.01$ in the time interval $[0, 70]$. Computational times (s) (median, minimum and maximum over 10 runs) and number of points required by PIRPNN, ode23s and ode15s with both absolute and relative tolerances set to $1e-03$ and $1e-06$. We note that most of the computational time for computing the solution with PIRPNN as shown, is due to the time required for the construction of the Jacobian matrix.

	$tol = 1e-03$				$tol = 1e-06$			
	median	min	max	# pts	median	min	max	# pts
PIRPNN	5.49e+00	5.19e+00	5.68e+00	330	6.37e+00	5.80e+00	7.53e+00	380
PIRPNN jac	4.41e+00	4.38e+00	4.45e+00		5.05e+00	4.44e+00	5.35e+00	
ode23s	1.03e-02	8.94e-03	1.88e-02	54	8.64e-02	8.35e-02	9.15e-02	529
ode15s	8.46e-03	7.87e-03	2.39e-02	68	1.67e-02	1.62e-02	2.32e-02	223
reference	2.35e-01	2.32e-01	2.56e-01	3706	2.41e-01	2.35e-01	2.76e-01	3706

the reference solution. As reported, the higher computational cost is due to the time required for the construction of the Jacobian matrix, which even if it is sparse has a complex structure that make difficult to assemble it in an efficient way. This task is beyond the scope of this paper. However, in a subsequent work, we aim at implementing matrix-free methods in the Krylov subspace [12, 41] such as Newton-GMRES for the solution of such large-scale problems.

3.7 Case Study 7: The Kuramoto-Sivashinsky PDE

The Kuramoto–Sivashinsky (KS) [70, 73] equation is a celebrated fourth-order nonlinear PDE which exhibits deterministic chaos. Here, we consider a one-dimensional formulation as proposed in [73]:

$$\frac{\partial u}{\partial t} = -uu_x - u_{xx} - u_{xxxx}, \quad x \in [0, 32\pi] \quad (50)$$

with periodic boundary condition and initial condition given by:

$$u(x, 0) = \cos\left(\frac{1}{16}x\right) \left(1 + \sin\left(\frac{1}{16}x\right)\right). \quad (51)$$

The integration time is [0 100]. To solve the KS PDE, we have used an equispaced grid in space using 201 points $x_1, x_2, \dots, x_{200}, x_{201}$, i.e., with a space step $dx = 32\pi/201$, and second order central finite difference, so that (50) became a system of 200 ODEs in the variables $u_i(t) = u(x_i, t)$:

$$\frac{\partial u_i}{\partial t} = -u_i \frac{u_{i+1} - u_{i-1}}{2dx} - \frac{u_{i+1} - 2u_i + u_{i-1}}{dx^2} - \frac{u_{i+2} - 4u_{i+1} + 6u_i - 4u_{i-1} + u_{i-2}}{dx^4} \quad (52)$$

$i = 1, \dots, 200.$

Here, as for the Allen-Cahn PDE, dealing with a resulting high dimensional Jacobian of size 4000×4000 , we have used a sparse QR decomposition as implemented in the SuiteSparseQR [18, 19]. Table 3.7 summarizes the approxima-

Table 13: Kuramoto-Shivasinsky PDE discretized with central FD (52) in the time interval [0 100]. Absolute errors (l^2 -norm, l^∞ -norm and MAE) for the solutions computed with both absolute and relative tolerances set to $1e-03$ and $1e-06$. The reference solution was computed with ode15s with tolerances equal to $1e-14$.

	$tol = 1e-03$			$tol = 1e-06$		
	l^2	l^∞	MAE	l^2	l^∞	MAE
RPNN	5.87e+01	5.77e+03	1.09e+04	8.20e-04	8.90e-06	1.29e-07
ode23s	9.40e+02	5.20e+00	2.40e+01	1.36e+01	1.39e-01	2.61e-03
ode15s	7.10e+01	4.87e+01	2.30e+02	2.38e-01	1.88e-03	7.69e-05

tion errors, in terms of l^2 -norm and l^∞ -norm errors and MAE, with respect to the reference solution in $100,000 \times 201$ equally spaced grid points in the time interval [0 100] and in the space interval [0 32π], respectively. As shown, for the given tolerances, the proposed method outperforms ode15s and ode23s in all metrics. As it is shown in Figure 8, for tolerances $1e-06$, the proposed scheme achieves more accurate solutions than ode23s and ode15s. In Table 3.7,

Table 14: Kuramoto-Shivasinsky PDE (52). Computational times in seconds (median, minimum and maximum over 10 runs) and number of points required in the time interval [0 100] by PIRPNN, ode23s and ode15s with both absolute and relative tolerances set to $1e-03$ and $1e-06$. The reference solution was computed by ode15s with tolerances equal to $1e-14$. We remark that most of the computational time for computing the solution with, reported in the row, is due to the time needed for the construction of the Jacobian, reported in the PIRPNN jac row, that for this problem has a dimension 4000×4000 .

	$tol = 1e-03$				$tol = 1e-06$			
	median	min	max	# pts	median	min	max	# pts
PIRPNN	8.81e+01	8.32e+01	9.47e+01	900	9.67e+01	9.13e+01	1.03e+02	1133
PIRPNN jac	8.29e+01	6.90e+01	8.66e+01		7.71e+01	7.59e+01	8.53e+01	
ode23s	1.38e+01	1.37e+01	1.65e+01	351	1.63e+00	1.59e+00	1.64e+00	4403
ode15s	3.22e+02	3.21e+02	4.45e+02	247	8.15e-02	7.43e-02	8.72e-02	749
reference	1.24e+00	1.21e+00	1.32e+00	14889	1.24e+00	1.21e+00	1.32e+00	14889

we report computational times and number of points required by each method, including the ones required for computing the reference solution. As shown, the corresponding total number of points required by the proposed scheme is comparable with the ones required by ode23s and ode15s and significantly less than the number of points required by the reference solution. On the other hand, the computing times of the proposed method are significantly larger than the ones concerning ode23s and ode15s (Table 3.7) and also with the ones required by the reference solution. As reported, the higher computational cost is due to the time required for the construction of the Jacobian matrix, which even if it is sparse has a complex structure that make difficult to assemble it. An efficient construction/assembly of the sparse Jacobian matrix is beyond the scope of this paper. However, in a subsequent work, we aim at implementing matrix-free methods in the Krylov subspace [12, 41] such as Newton-GMRES for the solution of such large-scale problems.

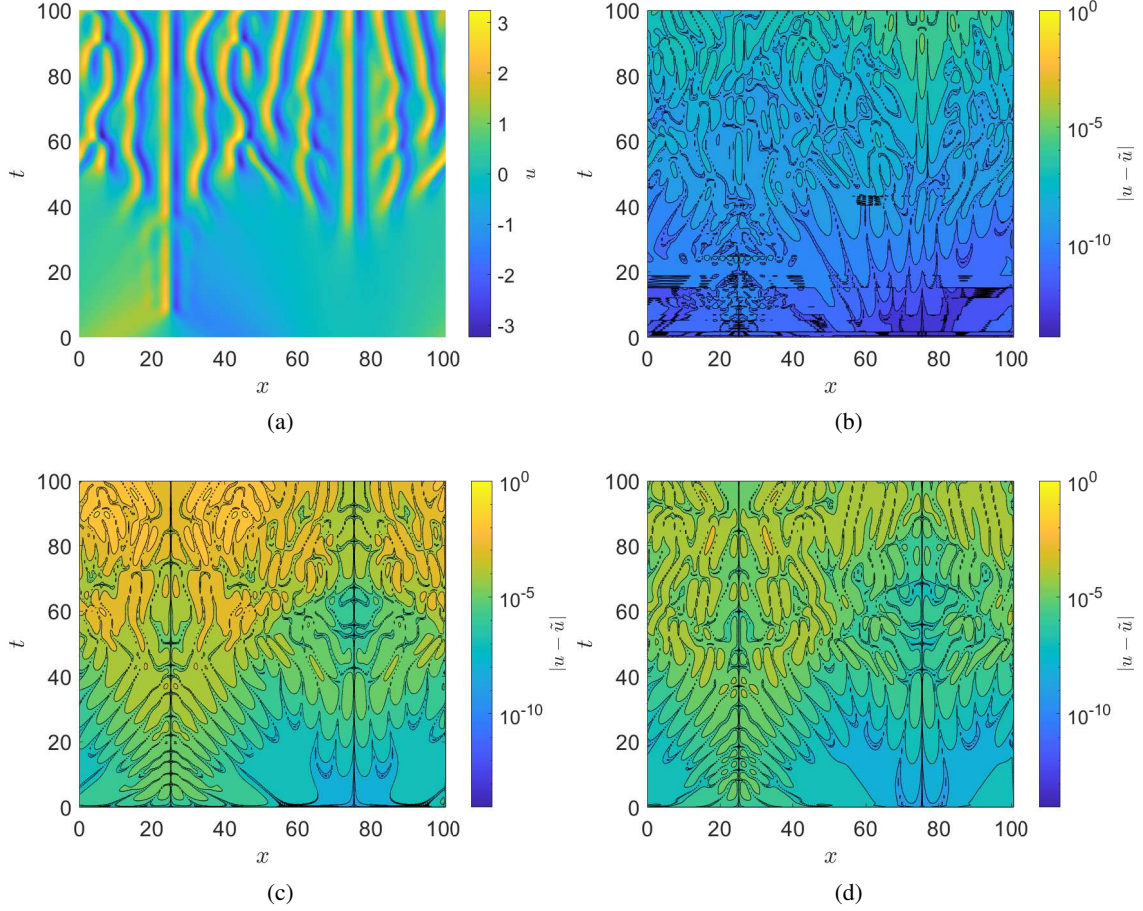


Figure 8: Kuramoto-Sivashinsky PDE discretized with FD (52) in the time interval $[0 \quad 100]$. Contour plots of absolute point error computed with tolerance $1e-06$: a) reference solution computed with ode15s with $tol=1e-14$, b) PIRPNN absolute errors c) ode23s absolute errors d) ode15s absolute errors.

4 Discussion

We proposed a physics-informed machine learning scheme based on the concept of random projections for the solution of IVPs of nonlinear ODEs and index-1 DAEs. The only unknowns are the weights from the hidden to the output layer which are estimated using Newton iterations. To deal with the ill-posedness least-squares problem, we used SVD decomposition when dealing with low-dimensional systems and sparse QR factorization with regularization when dealing with large-dimensional systems as for example those that arise from the discretization in space of PDEs. The hyper-parameters of the scheme, i.e., the bounds of the uniform distribution from which the values of the shape parameters of the Gaussian kernels are drawn and the interval of integration are parsimoniously chosen, based on the bias-variance trade-off concept and a variable step size scheme based on the elementary local error control algorithm. Furthermore, to facilitate the convergence of the scheme, we address a natural continuation method for providing good initial guesses for the Newton iterations.

The efficiency of the proposed scheme was assessed both in terms of numerical approximation accuracy and computation cost considering seven benchmark problems, namely the index-1 DAE Robertson model, a non autonomous index-1 DAEs mechanics problem, a non autonomous index-1 DAEs power discharge control problem, the chemical Akzo Nobel problem, the Belousov-Zhabotinsky ODEs model, the one-dimensional Allen-Cahn phase-field PDE and the one-dimensional Kuramoto-Sivashinsky PDE. In addition, the performance of the scheme was compared against three stiff solvers of the MATLAB ODE suite, namely the ode15s, ode23s and ode23t. The results suggest that proposed scheme arises an alternative method to well established traditional solvers.

Future work is focused on the further development and application of the scheme for solving very large scale stiff and DAE problems (also of index higher than one) arising in many problems of contemporary interest, thus considering and integrating ideas from other methods such as DASSL [55], CSP [31] and matrix-free methods in the Krylov-subspace [12, 41] in order to speed up computations for high-dimensional systems.

Acknowledgments

This work was supported by the Italian program “Fondo Integrativo Speciale per la Ricerca (FISR)” - FISR2020IP 02893/ B55F20002320001. G.F. is supported by a 4-year scholarship from the Scuola Superiore Meridionale, Università degli Studi di Napoli Federico II, Italy. E.G. was supported by a 3-year scholarship from the Università degli Studi di Napoli Federico II, Italy.

References

- [1] A. Alexandridis, C. Siettos, H. Sarimveis, A. Boudouvis, and G. Bafas. Modelling of nonlinear process dynamics using kohonen’s neural networks, fuzzy systems and chebyshev series. *Computers & Chemical Engineering*, 26(4-5):479–486, 2002.
- [2] S. M. Allen and J. W. Cahn. A microscopic theory for antiphase boundary motion and its application to antiphase domain coarsening. *Acta metallurgica*, 27(6):1085–1095, 1979.
- [3] H. Arbabi, J. E. Bunder, G. Samaey, A. J. Roberts, and I. G. Kevrekidis. Linking machine learning with multiscale numerics: Data-driven discovery of homogenized equations. *Jom*, 72(12):4444–4457, 2020.
- [4] A. R. Barron. Universal approximation bounds for superpositions of a sigmoidal function. *IEEE Transactions on Information theory*, 39(3):930–945, 1993.
- [5] A. G. Baydin, B. A. Pearlmutter, A. A. Radul, and J. M. Siskind. Automatic differentiation in machine learning: a survey. *Journal of machine learning research*, 18, 2018.
- [6] M. Belkin, D. Hsu, S. Ma, and S. Mandal. Reconciling modern machine-learning practice and the classical bias–variance trade-off. *Proceedings of the National Academy of Sciences*, 116(32):15849–15854, 2019.
- [7] B. P. Belousov. A periodic reaction and its mechanism. *Oscillation and Travelling Waves in Chemical Systems*, 1951.
- [8] R. Belusov. Periodically acting reaction and its mechanism. *Collection of Abstracts on Radiation Medicine (in Russian)*, 1959.
- [9] T. Bertalan, F. Dietrich, I. Mezić, and I. G. Kevrekidis. On learning hamiltonian systems from data. *Chaos: An Interdisciplinary Journal of Nonlinear Science*, 29(12):121107, 2019.
- [10] J. Bongard and H. Lipson. Automated reverse engineering of nonlinear dynamical systems. *Proceedings of the National Academy of Sciences*, 104(24):9943–9948, 2007.
- [11] K. E. Brenan, S. L. Campbell, and L. R. Petzold. *Numerical solution of initial-value problems in differential-algebraic equations*. SIAM, 1995.
- [12] P. N. Brown, A. C. Hindmarsh, and L. R. Petzold. Using krylov methods in the solution of large-scale differential-algebraic systems. *SIAM Journal on Scientific Computing*, 15(6):1467–1488, 1994.
- [13] F. Calabrò, G. Fabiani, and C. Siettos. Extreme learning machine collocation for the numerical solution of elliptic PDEs with sharp gradients. *Computer Methods in Applied Mechanics and Engineering*, 387:114188, 2021.
- [14] T. Chen and H. Chen. Universal approximation to nonlinear operators by neural networks with arbitrary activation functions and its application to dynamical systems. *IEEE Transactions on Neural Networks*, 6(4):911–917, 1995.
- [15] W. Chen, Q. Wang, J. S. Hesthaven, and C. Zhang. Physics-informed machine learning for reduced-order modeling of nonlinear problems. *Journal of Computational Physics*, 446:110666, 2021.
- [16] Y. Chen, B. Hosseini, H. Owjadi, and A. M. Stuart. Solving and learning nonlinear pdes with gaussian processes. *Journal of Computational Physics*, 447:110668, 2021.
- [17] P. Collins and O. U. K. M. Inst;. *Differential and Integral Equations: Part II*. University of Oxford Mathematical Institute, 1988.
- [18] T. A. Davis. User’s guide for suitesparseqr, a multifrontal multithreaded sparse qr factorization package, 2009.
- [19] T. A. Davis. Algorithm 915, suitesparseqr: Multifrontal multithreaded rank-revealing sparse qr factorization. *ACM Transactions on Mathematical Software (TOMS)*, 38(1):1–22, 2011.

- [20] N. De Villiers and D. Glasser. A continuation method for nonlinear regression. *SIAM Journal on Numerical Analysis*, 18(6):1139–1154, 1981.
- [21] M. Dissanayake and N. Phan-Thien. Neural-network-based approximations for solving partial differential equations. *communications in Numerical Methods in Engineering*, 10(3):195–201, 1994.
- [22] S. Dong and Z. Li. Local extreme learning machines and domain decomposition for solving linear and nonlinear partial differential equations. *Computer Methods in Applied Mechanics and Engineering*, 387:114129, 2021.
- [23] S. Dong and Z. Li. A modified batch intrinsic plasticity method for pre-training the random coefficients of extreme learning machines. *Journal of Computational Physics*, 445:110585, 2021.
- [24] G. Fabiani, F. Calabrò, L. Russo, and C. Siettos. Numerical solution and bifurcation analysis of nonlinear partial differential equations with extreme learning machines. *Journal of Scientific Computing*, 89:44, 2021.
- [25] C. Gear. An introduction to numerical methods for odes and daes. In *Real-time integration methods for mechanical system simulation*, pages 115–126. Springer, 1990.
- [26] C. W. Gear. Numerical initial value problems in ordinary differential equations. *Prentice-Hall series in automatic computation*, 1971.
- [27] R. Gerstberger and P. Rentrop. Feedforward neural nets as discretization schemes for ODEs and DAEs. *Journal of Computational and Applied Mathematics*, 82(1-2):117–128, 1997.
- [28] I. Gladwell, L. Shampine, and R. Brankin. Automatic selection of the initial step size for an ode solver. *Journal of computational and applied mathematics*, 18(2):175–192, 1987.
- [29] R. González-García, R. Rico-Martinez, and I. G. Kevrekidis. Identification of distributed parameter systems: A neural net based approach. *Computers & chemical engineering*, 22:S965–S968, 1998.
- [30] A. N. Gorban, I. Y. Tyukin, D. V. Prokhorov, and K. I. Sofeikov. Approximation with random bases: Pro et contra. *Information Sciences*, 364:129–145, 2016.
- [31] M. Hadjinicolaou and D. A. Goussis. Asymptotic solution of stiff pdes with the csp method: the reaction diffusion equation. *SIAM Journal on Scientific Computing*, 20(3):781–810, 1998.
- [32] E. Hairer, S. P. Norsett, and G. Wanner. *Solving Ordinary, Differential Equations I, Nonstiff problems, with 135 Figures, Vol.: 1*. 2Ed. Springer-Verlag, 2000, 2000.
- [33] G.-B. Huang. An insight into extreme learning machines: random neurons, random features and kernels. *Cognitive Computation*, 6(3):376–390, 2014.
- [34] G.-B. Huang, Q.-Y. Zhu, and C.-K. Siew. Extreme learning machine: theory and applications. *Neurocomputing*, 70(1-3):489–501, 2006.
- [35] D. Husmeier. Random vector functional link (RVFL) networks. In *Neural Networks for Conditional Probability Estimation*, pages 87–97. Springer, 1999.
- [36] B. Igelnik and Y.-H. Pao. Stochastic choice of basis functions in adaptive function approximation and the functional-link net. *IEEE Transactions on Neural Networks*, 6(6):1320–1329, 1995.
- [37] H. Jaeger. Adaptive nonlinear system identification with echo state networks. *Advances in Neural Information Processing Systems*, 15:609–616, 2002.
- [38] W. Ji, W. Qiu, Z. Shi, S. Pan, and S. Deng. Stiff-pinn: Physics-informed neural network for stiff chemical kinetics. *The Journal of Physical Chemistry A*, 125(36):8098–8106, 2021.
- [39] W. B. Johnson and J. Lindenstrauss. Extensions of Lipschitz mappings into a Hilbert space. *Contemporary Mathematics*, 26(1):189–206, 1984.
- [40] G. E. Karniadakis, I. G. Kevrekidis, L. Lu, P. Perdikaris, S. Wang, and L. Yang. Physics-informed machine learning. *Nature Reviews Physics*, 3(6):422–440, 2021.
- [41] C. T. Kelley. *Iterative methods for optimization*. SIAM, 1999.
- [42] K. Krischer, R. Rico-Martinez, I. G. Kevrekidis, H. Rotermund, G. Ertl, and J. Hudson. Model identification of a spatiotemporally varying catalytic reaction. *Aiche Journal*, 39(1):89–98, JAN 1993 1993.
- [43] Y. Kuramoto. Diffusion-induced chaos in reaction systems. *Progress of Theoretical Physics Supplement*, 64:346–367, 1978.
- [44] I. E. Lagaris, A. Likas, and D. I. Fotiadis. Artificial neural networks for solving ordinary and partial differential equations. *IEEE Transactions on Neural Networks*, 9(5):987–1000, 1998.
- [45] H. Larochelle, Y. Bengio, J. Louradour, and P. Lamblin. Exploring strategies for training deep neural networks. *Journal of machine learning research*, 10(1), 2009.

- [46] H. Lee and I. S. Kang. Neural algorithm for solving differential equations. *Journal of Computational Physics*, 91(1):110–131, 1990.
- [47] S. Lee, M. Kooshkbaghi, K. Spiliotis, C. I. Siettos, and I. G. Kevrekidis. Coarse-scale pdes from fine-scale observations via machine learning. *Chaos: An Interdisciplinary Journal of Nonlinear Science*, 30(1):013141, 2020.
- [48] L. Lu, P. Jin, G. Pang, Z. Zhang, and G. E. Karniadakis. Learning nonlinear operators via deeponet based on the universal approximation theorem of operators. *Nature Machine Intelligence*, 3(3):218–229, 2021.
- [49] L. Lu, X. Meng, Z. Mao, and G. E. Karniadakis. DeepXDE: a deep learning library for solving differential equations. *SIAM Review*, 63(1):208–228, 2021.
- [50] S. F. Masri, A. G. Chassiakos, and T. K. Caughey. Identification of nonlinear dynamic systems using neural networks. *Journal of Applied Mechanics*, 60(1):123–133, 03 1993.
- [51] F. Mazzia, J. R. Cash, and K. Soetaert. A test set for stiff initial value problem solvers in the open source software R: Package detestset. *Journal of Computational and Applied Mathematics*, 236(16):4119–4131, 2012.
- [52] A. J. Meade Jr and A. A. Fernandez. The numerical solution of linear ordinary differential equations by feedforward neural networks. *Mathematical and Computer Modelling*, 19(12):1–25, 1994.
- [53] X. Meng, Z. Li, D. Zhang, and G. E. Karniadakis. PPINN: parareal physics-informed neural network for time-dependent PDEs. *Computer Methods in Applied Mechanics and Engineering*, 370:113250, 2020.
- [54] L. Métivier and P. Montarnal. Strategies for solving index one dae with non-negative constraints: Application to liquid–liquid extraction. *Journal of Computational Physics*, 231(7):2945–2962, 2012.
- [55] L. R. Petzold. Description of dassl: a differential/algebraic system solver. Technical report, Sandia National Labs., Livermore, CA (USA), 1982.
- [56] A. Rahimi and B. Recht. Weighted sums of random kitchen sinks: replacing minimization with randomization in learning. In *Nips*, pages 1313–1320. Citeseer, 2008.
- [57] M. Raissi, P. Perdikaris, and G. E. Karniadakis. Machine learning of linear differential equations using gaussian processes. *Journal of Computational Physics*, 348:683–693, 2017.
- [58] M. Raissi, P. Perdikaris, and G. E. Karniadakis. Numerical Gaussian processes for time-dependent and nonlinear partial differential equations. *SIAM Journal on Scientific Computing*, 40(1):A172–A198, 2018.
- [59] M. Raissi, P. Perdikaris, and G. E. Karniadakis. Physics-informed neural networks: A deep learning framework for solving forward and inverse problems involving nonlinear partial differential equations. *Journal of Computational Physics*, 378:686–707, 2019.
- [60] H. Robertson. The solution of a set of reaction rate equations. *Numerical Analysis: an Introduction*, 178182, 1966.
- [61] F. Rosenblatt. *Perceptions and the theory of brain mechanisms*. Spartan books, 1962.
- [62] S. Rudy, A. Alla, S. L. Brunton, and J. N. Kutz. Data-driven identification of parametric partial differential equations. *SIAM Journal on Applied Dynamical Systems*, 18(2):643–660, 2019.
- [63] E. Schiassi, R. Furfaro, C. Leake, M. De Florio, H. Johnston, and D. Mortari. Extreme theory of functional connections: A fast physics-informed neural network method for solving ordinary and partial differential equations. *Neurocomputing*, 457:334–356, 2021.
- [64] L. F. Shampine and C. W. Gear. A user’s view of solving stiff ordinary differential equations. *SIAM review*, 21(1):1–17, 1979.
- [65] L. F. Shampine and M. W. Reichelt. The MATLAB ODE suite. *SIAM Journal on Scientific Computing*, 18(1):1–22, 1997.
- [66] L. F. Shampine, M. W. Reichelt, and J. A. Kierzenka. Solving index-1 daes in matlab and simulink. *SIAM review*, 41(3):538–552, 1999.
- [67] V. Shulyk, O. Klymenko, and I. Svir. Numerical solution of stiff odes describing complex homogeneous chemical processes. *Journal of mathematical chemistry*, 43(1), 2008.
- [68] C. I. Siettos and G. V. Bafas. Semiglobal stabilization of nonlinear systems using fuzzy control and singular perturbation methods. *Fuzzy Sets and Systems*, 129(3):275–294, 2002.
- [69] C. I. Siettos, G. V. Bafas, and A. G. Boudouvis. Truncated chebyshev series approximation of fuzzy systems for control and nonlinear system identification. *Fuzzy sets and systems*, 126(1):89–104, 2002.

- [70] G. I. Sivashinsky. Nonlinear analysis of hydrodynamic instability in laminar flames—i. derivation of basic equations. *Acta astronautica*, 4(11):1177–1206, 1977.
- [71] G. Söderlind. Automatic control and adaptive time-stepping. *Numerical Algorithms*, 31(1):281–310, 2002.
- [72] W. J. H. Stortelder et al. *Parameter estimation in nonlinear dynamical systems*. CWI Amsterdam, The Netherlands, 1998.
- [73] L. N. Trefethen. *Spectral methods in MATLAB*. SIAM, 2000.
- [74] P. R. Vlachas, J. Pathak, B. R. Hunt, T. P. Sapsis, M. Girvan, E. Ott, and P. Koumoutsakos. Backpropagation algorithms and reservoir computing in recurrent neural networks for the forecasting of complex spatiotemporal dynamics. *Neural Networks*, 126:191–217, 2020.
- [75] S. Wang, Y. Teng, and P. Perdikaris. Understanding and mitigating gradient flow pathologies in physics-informed neural networks. *SIAM Journal on Scientific Computing*, 43(5):A3055–A3081, 2021.
- [76] S. Wang, X. Yu, and P. Perdikaris. When and why pinns fail to train: A neural tangent kernel perspective. *Journal of Computational Physics*, 449:110768, 2022.
- [77] A. M. Zhabotinsky. Periodical oxidation of malonic acid in solution (a study of the belousov reaction kinetics). *Biofizika*, 9:306–311, 1964.